Crustal-upper mantle velocity structure from the North Qilian Shan to ~~Beishan block~~Beishan Orogenic Collage and the tectonic significance of ~~the~~ crustal deformation

Xiaosong Xiong [1*], Yingkang Li[2], Xuanhua Chen[1], Guowei Wu[1], Rui Gao[3], Jennifer D. Eccles[4]

1 State Key Laboratory of Deep Earth and Mineral Exploration, Chinese Academy of Geological Sciences, Beijing~~,~~ 100094, China

2 Geological Cores and Samples of Natural Resources, CGS, Sanhe, 065201, China

3 School of Earth Science and Geological Engineering, Sun Yat-sen University, Guangzhou 510275, China

4 School of Environment, University of Auckland, Auckland 1142, New Zealand

* Corresponding author: Xiaosong Xiong (benxung@126.com)

Abstract The Qilian Shan ~~constitutes~~ represents a Cenozoic fold-thrust belt characterized by multi-stage tectonic deformation since the Paleozoic. North of it lies the ~~The~~ Hexi corridor basins and the Beishan ~~block~~orogenic belt, which constitute~~, located north of the Qilian Shan, are~~ the southern segment of the Central Asian Orogenic Belt~~.~~. The crustal-mantle structure of the study area, ~~serves as~~ a transition zone, is crucial ~~for comprehending~~to understanding the deep processes of accretion and crustal deformation. This study ~~introduces~~ presents a newly acquired 460-km ~~seismic~~ wide~~-~~angle reflection and refraction profile ~~spanning~~ traversing from the North Qilian Shan to the ~~Beishan block~~Beishan Orogenic Collage (BOC). ~~The~~ P-wave velocity structure ~~of the crust and upper mantle indicates~~reveals a 47.5–60 km thick crust ~~crustal thickness between 47.5 km and 60 km, segmented~~divided into five ~~strata~~layers. The deepest Moho (60 km) lies beneath the central Jiuquan ~~basin displays the most substantial crust, measuring 59.5–60 km in thickness~~. ~~The~~ Average crustal velocities (6.24–6.43 km s^{-1})~~y varies between 6.24 and 6.43 km/s, while the~~and Pn values~~velocity~~ ~~(ranges from~~ 7.7 ~~km/s~~–~~to~~ 8.1 ~~km/s~~km s^{-1}) reveal strong lateral~~. The considerable variance in crustal velocity indicates~~ heterogeneity. North-dipping velocity contours from 20 km to the uppermost mantle beneath the Qilian Shan, coupled with a lower-crust–upper-mantle low-velocity corridor beneath the Hexi Basin, support early Paleozoic north-dipping subduction of the Qilian Ocean. A positive upper-mantle anomaly (8.0–8.3 km s^{-1}, 45–70 km depth) aligns with the Hongliuhe–Xichangjing ophiolite mélange likely represents a fossil ~~break-off~~ slab broken off after north-dipping subduction of the Beishan Ocean. Crustal velocity contrasts across the southern margin fault of the Beishan affirm its role as a regional strike-slip structure. Integrating geological and geophysical evidence, we suggest that the Altyn Tagh Fault does not terminate at the Qilian Shan front but rather extends east-northeast along the southern margin of the BOC into the Beishan and Alxa Block.

~~in the crustal composition of the Qilian Shan and Beishan block. The southern edge fault of the Beishan block delineates the area, where northward and southward thrusting induces upper crustal deformation on opposing sides. The crust of the southern Beishan block is weaker than that of the bordering regions. Additionally, we propose a north-direction subduction polarity of the Qilian Ocean based on the northward-tilted velocity contour in Paleozoic.~~

Keywords: North Qilian; ~~Beishan Block~~Beishan Orogenic Collage; Altyn T~~t~~agh fault; Crustal-upper mantle velocity structure~~; crustal deformation~~

The NW-SE-trending Qilian Shan, situated in the NE Tibet, is bounded by the Altyn Tagh fault (ATF) to the west, the northern Qaidam thrust system to the south, the Haiyuan fault to the east, and the north Qilian Shan fault to the north (Fig. 1b). The present-day Qilian Shan exhibits a Cenozoic fold-thrust belt with~~enduring~~ multi-stage tectonic deformation prior to the Cenozoic (Yin and

样式定义: 正文
设置了格式: 字体: 倾斜, 非上标/ 下标
设置了格式: 字体: 倾斜
带格式的: 行距: 多倍行距 1.15 字行
设置了格式: 字体: 倾斜, 非上标/ 下标
设置了格式: 字体: 倾斜
设置了格式: 字体: 倾斜, 非上标/ 下标
设置了格式: 字体: 倾斜
设置了格式: 字体: 倾斜, 非上标/ 下标
设置了格式: 字体: 倾斜
设置了格式: 字体: Times New Roman, 10.5 磅, 非倾斜, 字体颜色: 自动设置
设置了格式: 字体: Times New Roman, 10.5 磅, 非倾斜, 字体颜色: 自动设置
设置了格式: 字体: 10.5 磅
设置了格式: 上标
设置了格式: 上标

Harrison 2000; Gehrels et al. 2003; Song et al. 2014; Wu et al. 2016; Zuza et al. 2017; 2019)~~.~~. ~~The Qilian Shan exhibits a Cenozoic fold-thrust belt with multi-stage tectonic deformation since Paleozoic.~~ North of the Qilian Shan, the Hexi corridor basins and the ~~Beishan block~~Beishan Orogenic Collage (BOC) form the southern section of the Central Asian Orogenic Belt (CAOB, Xiao et al., 2010; Li et al., 2023; Xiong et al., 2024). As the middle of the South Tienshan-Beishan-Solonker suture zone, the BOC underwent multi-stage breakup, subduction, collision, and amalgamation during the closure of the Paleo-Asian Ocean (PAO)~~AO~~, mainly in the Paleozoic (Fig. 1; Zuo et al. 1991; Liu 1995; Yue and Liou 1999; Wang et al. 2010; Xiao et al. 2010; Zuo and Li 2011; Şengör 2015; ~~Liu 1995;~~ Yuan et al. 2015; He et al. 2018; Li et al. 2023). The geological history of the BOC is further complicated by regional extension, subsequent intracontinental overthrusting, and strike-slip faulting since Mesozoic (Zheng et al. 1996; Meng et al., 2003; Xiao et al. 2010; Zuo and Li 2011; Zhang and Cunningham 2012; Li et al. 2023). ~~is inside the middle of the South Tienshan-Beishan-Solonker suture zone (Fig. 1b).~~Particularly in the Cenozoic, the far-field effect of the Indian-Eurasian collision led to the outward expansion of the NE Tibetan Plateau, and reactivated the Qilian Shan, causing stress to propagate across the Hexi corridor basins into the BOC, and extending even further north to the Mongolian Plateau (Cunningham 2013; Zheng et al. 2017; Wang et al. 2022).

The Qilian Shan is~~became~~ an important part of the Tibetan plateau, playing a significant role in accommodating~~researching~~ the intracontinental convergence, thrusting-folding and the northern extension of ~~The~~ NE Tibet (Meyer et al. 1998; Yuan et al. 2013; Zuza et al. 2017). As the southernmost CAOB, the BOC acted as a major zone~~area for examining the~~ for the reactivation of inherited structures ~~the ancient crust~~ during~~and~~ the transmission of compressional stress leading to the uplift~~outward exhumation~~ of the NE Tibetan and ~~the~~ Mongolian Plateaus in Cenozoic. Therefore, a~~Acting a~~s ~~a~~ the transition zone between the NE Tibetan Plateau and CAOB, the crustal-mantle structure of the ~~studied~~ study area is crucial for ~~comprehending~~ understanding the regional evolution and interaction of ~~including the Qilian Shan and Beishan block operates as the contact zone between the northeastern Tibetan plateau~~Tibetan Plateau, ~~(NE Tibet) and the southern CAOB. This region acts as the transition zone between~~ the Tethys tectonic domain and the ~~Paleo-Asian ocean~~PAO~~ic (PAO)~~ tectonic domain ~~(PAO)~~ since the Paleozoic (Fig. 1a; Li et al. 1982; Yin and Harrison 2000; Xiao et al. 2009; Zhao et al. 2018).

Previous geophysical studies across the Qilian Shan–BOC transition zone, have provided valuable insights into the subduction polarity, continental extension, lithospheric foundering and magmatic activity (Xiao et al. 2012; Huang et al. 2014; Wei et al. 2017; Xu et al. 2019; Shen et al. 2020; Huang et al. 2021; Yang et al. 2024). Nevertheless, the crustal-upper mantle velocity structure remains ambiguous because earlier acquisition methods and parameters limited resolution. In this study, we present a 460-km-long, SW-NE-trending wide-angle reflection and refraction profile that traverses the North Qilian Shan, Hexi corridor (containing the Jiuquan basin and the Huahai basin), and the entire BOC. The new data yield a high-quality crustal-upper mantle velocity structure of the study area. Combined with existing geological and geophysical evidence, we discuss the tectonic significance of the transition zone, provide new constraints of the subduction polarity of the Qilian Ocean and the southern PAO, elucidate the crustal deformation mechanism across main regional faults, and propose the eastern termination and extension of the ATF.~~The NW-SE trending Qilian Shan, situated in NE Tibet, is bordered by the Altyn Tagh fault to the west, the northern Qaidam thrust system to the south, the Haiyuan fault to the east, and the north Qilian Shan fault to the north (Figure 1b). The present-day Qilian Shan has witnessed Cenozoic reactivation as a fold-thrust belt (Zuza et al. 2017, 2019), enduring multi-stage tectonic deformation prior to the Cenozoic (Yin and Harrison 2000; Gehrels et al. 2003; Song et al. 2014; Wu et al. 2016; Zuza et al. 2017). The Beishan block, sometimes referred to as the Beishan orogenic belt (Liu 1995; Yuan et al. 2015; He et al. 2018; Li et al. 2023), is inside the middle of the South Tienshan-Beishan-Solonker suture zone (Fig. 1b). Experiencing multi-stage breakup, subduction, collision, and amalgamation during the closure of the PAO, mainly in the Paleozoic (Fig. 1; Zuo et al. 1991; Yue and Liou 1999; Wang et al. 2010; Xiao et al. 2010; Zuo and Li 2011; Şengör 2015), the geological history of the Beishan block is further complicated by regional extension overlap, subsequent intracontinental overthrusting, and strike-slip faulting since Mesozoic (Zheng et al. 1996; Xiao et al. 2010; Zuo and Li 2011; Zhang and Cunningham 2012; Li et al. 2023). The NE-trending grabens in the Gobi Altai, southeastern Mongolia and Beishan forms a rift system, associated with the termination of the final subduction of the PAO (Meng 2003; Donskaya et al. 2008; Cunningham et al. 2009; Davis and Darby 2010) or~~

带格式的: 缩进: 首行缩进: 0 字符

the Cenozoic Indian-Eurasian collision (Zhang et al. 2007, 2021; Buslov 2012). This study proposes a new-acquired 460-km-long seismic wide-angle and refraction profile encompassing the North Qilian Shan to Beishan block. The crustal-upper mantle P-wave velocity structure reveals the crustal thickness ranging from 47.5 to 60 km, divided into five layers. The central Jiuquan basin has the thickest crust at 59.5–60 km. Average crustal velocity ranges from 6.24 to 6.43 km/s, and Pn velocity of 7.7–8.1 km/s. Notably, the considerable variance in crustal velocity shows inhomogeneity non the crustal composition of the Qilian Shan and Beishan block. Bounded by the southern edge fault of the Beishan block, north-direction and south-direction thrusting contribute to upper crustal deformation to separate sides. The crust of the southern Beishan block is weaker than that of the bordering regions. Additionally, we propose a north-direction subduction polarity of the Qilian Ocean based on the northward-tilted velocity contour in Paleozoic.

In Cenozoic, the far-field effect of the Indian-Eurasian collision led to the outward expansion of NE Tibet, spreading across the Hexi corridor basins into the Beishan block or the Mongolian Altai Mountains (Mts.) (Cunningham 2013; Zheng et al. 2017; Wang et al. 2022). The reactivated Qilian Shan finally became an important part of the Tibet plateau, playing a significant role in researching the intracontinental convergence, thrusting-folding and the northern extension of NE Tibet (Meyer et al. 1998; Yuan et al. 2013; Zuza et al. 2017). As the southernmost CAOB, the Beishan block also served as a major place for examining the reactivation of the ancient crust and the transmission of compressional stress arising from the outward exhumation of NE Tibet and the Mongolian plateau in Cenozoic.

While previous geophysical studies have been conducted in the Qilian Shan - Beishan block transition zone to comprehend the subduction polarity, continental extension, foundering and magmatic activities (Xiao et al. 2012; HUANG et al. 2014; Wei et al. 2017; Xu et al. 2019; Shen et al. 2020; Huang et al. 2021; Yang et al. 2024), the crustal-upper mantle structure remains ambiguous due to limited resolution quality. In this study, a N-S-trending 460-km-long seismic wide-angle and refraction profile sweeps throughout the North Qilian, Hexi corridor (containing the Jiuquan basin and the Huahai basin), and the entire Beishan block was done. This profile reflects the high-quality crustal-upper mantle velocity structure of the research area. Combined with other geological and geophysical datasets, we examined the tectonic consequence of the key characteristics of the velocity structure, hoping to throw light on the northern extension of the NE Tibet plateau, and the reactivation of the Beishan crust.

Geological Ssetting

The early Paleozoic Qilian Shan, recording the closure of the Qilian Ocean as part of the Proto-Tethys Ocean (Yu et al. 2021), has beenis a typical orogen traditionally divided into three structural units: the North Qilian Shan Orogenic belt (NQS), the Central Qilian block, and the South Qilian thrust belt (Yin and Harrison 2000). The boundary between the former two units is delimited by the North Qilian fault (F9). The NQS principally comprises early Paleozoic ophiolite suites (Fig. 1c), blueschists, eclogites, greenschists, and arc-related magmatic and volcanic rocks (Xu et al. 2005; Zhang et al. 2007; Song et al. 2009; Xiao et al. 2009; Zhao et al. 2024). These strata are overlain by Silurian flysch, Devonian molasse and Carboniferous-Triassic sedimentary periods (Wang et al. 2023). In the Mesozoic, the extensional and transtensional basins evolved over the Qilian Shan from the Xining Basin in the south to the Hexi corridor in the north (Horton et al. 2004; Pan et al. 2004). In the Cenozoic, the Qilian Shan has been reactivated as a fold-thrust belt to accommodate the crustal deformation resultant from the Indian-Eurasian collision with development of massive thrusts and strike-slip faults (Tapponnier et al. 1990; Zuza et al. 2019).

The Hexi corridor, sandwiched between the BOC and the Qilian Shan by the southern margin fault of the Beishan (F5) and northern margin fault of the North Qilian (F8), is a Cenozoic foreland basin system (Fig. 1b; Li et al. 2002). The basement of the Hexi corridor consists predominantly Paleozoic rocks, covered by thick Mesozoic and Cenozoic deposits. In this study region, tThe Hexi corridor is divided into the Huahai basin in the north and Jiuquan basin in the south by the Kuantanshan-Heishan fault (F6). The Huahai basin is part of the Dunhuang block, traditionally assigned as a Precambrian cratonic block or a microcontinent (BGMRGP 1989; Che and Sun 1996; Mei et al. 1997; Mei 1998; Yu et al. 1998; Ren et al. 1999; Xu et al. 1999; Lu et al. 2008; Liu et al. 2009; Zhang et al. 2011; He et al. 2013; Zong et al. 2013), and involved in the final closurecollision of the PAO~~aleo-Asian Ocean~~ (~~PAO, ~~Shi et al. 2022). The Jiuquan basin, a subbasin of the Hexi Corridor foreland basin, has ~~deposited ~~Cenozoic sediments deposited since as early as ca. 40 Ma (Dai et al. 2005; Wang et al. 2016), and was subsequently influenced by the uplift of the NQS since Cenozoic.

The ~~Beishan block~~BOC is positioned between the Mongolian Plateau ~~collage system ~~in the north and the Dunhuang Block in the south (Fig. 1; Zuo et al. 1991; Yue and Liou 1999; Wang et al. 2010; Xiao et al. 2010; Zuo and Li 2011). It is widely considered to encompass multiple different ~~volcani~~islande??? ~~terrane~~arcs, including the Que'ershan, Hanshan, Mazongshan, Shuangyingshan, and Shibanshan ~~terrane~~arcs. They are separated by four nearly parallel W-E-trending ophiolite mélange zones, named Hongshishan-Baiheshan (F1), Shibanjing-Xiaohuangshan (F2), Hongliuhe-Xichangjing (F3) and Liuyuan-Huitongshan-Zhangfangshan (F4) ~~respectively ~~(Fig. 1c; Zuo et al. 1991; Liu 1995; Wei et al. 2004; Ao et al. 2010, 2012, 2016; Xiao et al. 2010; Yang et al. 2010; Zuo and Li 2011; He et al. 2014; Wang et al. 2017; Wei et al. 2017; He et al. 2018; Wang et al. 2018; Li et al. 2022; Li et al. 2023). The Hongliuhe-Xichangjing suture zone (F3) is generally recognized as the final a~~sealing ~~malgamation position~~position~~ of the South ~~Beishan Block~~BOC and North ~~Beishan block~~BOC in the middle to ~~-~~late Ordovician ~~-~~(Li et al. 2022).

~~The Hexi corridor, sandwiched between the Beishan block and the Qilian Shan by the southern margin fault of the Beishan (F5) and northern margin fault of the North Qilian (F8), is a Cenozoic foreland basin system (Fig. 1b; Li et al. 2002). The basement of the Hexi corridor consists predominantly Paleozoic rocks, covered by thick Mesozoic and Cenozoic deposits. In this study region, The Hexi corridor is divided into the Huahai basin in the north and Jiuquan basin in the south by the Kuantanshan-Heishan fault (F6). The Huahai basin is part of the Dunhuang block, traditionally assigned as a Precambrian cratonic block or a microcontinent (BGMRGP 1989; Che and Sun 1996; Mei et al. 1997; Mei 1998; Yu et al. 1998; Ren et al. 1999; Xu et al. 1999; Lu et al. 2008; Liu et al. 2009; Zhang et al. 2011; He et al. 2013; Zong et al. 2013), and involved in the final collision of the PAO (Shi et al. 2022). The Jiuquan basin, a subbasin of the Hexi Corridor foreland basin, has deposited Cenozoic sediments since as early as ca. 40 Ma (Dai et al. 2005; Wang et al. 2016), and was subsequently influenced by the uplift of the North Qilian since Cenozoic. The early Paleozoic Qilian Shan, recording the closure of the Qilian Ocean as part of the Proto-Tethys Ocean (Yu et al. 2021), is a classic orogen traditionally divided into three structural units: the North Qilian Shan Orogenic belt (NQS), the Central Qilian block, and the South Qilian thrust belt (Yin and Harrison 2000). The previous two units are delimited by the North Qilian fault (F9). The NQS principally comprises early Paleozoic ophiolite suites (Fig. 1c), blueschists, eclogites, greenschists, and arc-related magmatic and volcanic rocks (Xu et al. 2005; Zhang et al. 2007; Song et al. 2009; Xiao et al. 2009; Zhao et al. 2024). These strata are overlain by Silurian flysch, Devonian molasse and Carboniferous-Triassic sedimentary periods (Wang et al. 2023). In Mesozoic, the extensional and transtensional basins evolved over the Qilian Shan from the Xining Basin in the south to the Hexi corridor in the north (Horton et al. 2004; Pan et al. 2004). In Cenozoic, the Qilian Shan has been reactivated as a fold-thrust belt to accommodate the crustal deformation resultant from the Indian-Eurasian collision with development of massive thrusts and strike-slip faults (Tapponnier et al. 1990; Zuza et al. 2019).~~

Data and M~~m~~ethods

S~~s~~eismic Acquisition~~collection and processing~~

In 2018, The Chinese Academy of Geological Sciences collecte~~mplete~~d a SW-NE-trending ~~seismic ~~wide-angle reflection and refraction profile stretching from the ~~North Qilian~~NQS to the ~~Beishan block~~BOC. The profile starts from Yanglong in Qinghai Province in the south, passing through Qingqing, Baiyanghe, Dongxiang Ethnic Town, Ganhaizi, Humuletu Wusu, Sharitaolai, Wutongjing, Heiyingshan, and Har Borogdyn Uul, before ending at the China-Mongolia border in the north. Nine ~~TNT ~~trinitrotoluene (TNT) ~~blasts~~shots, ranging from 1.5 to 3.0 tons, were detonated~~exploded~~ throughout the seismic profile at intervals of~~ roughly~~ 30–60 km (ZB0–ZB8, shown in red stars in Fig. 1c). To ~~achieve thorough~~ensure dense ray coverage, 250 portable seismographs (depicted as blue circles in Fig. 1c) were ~~strategically distributed~~deployed along the ~~whole ~~entire seismic line~~profile~~ at a spacing of 2–3 km. T~~his deployment sought to capture high-~~

~~quality seismic data, and t~~the ~~specific~~ detailed parameters of the shots are presented in Table 1.

Identification of S~~S~~eismic P~~p~~hases

Using the ZPLOT plotting package (Zelt, 1994), we performed trace editing, automatic gain control, band-pass filtering, velocity reduction, and phase picking for each shot. To ~~make the seismic records clearer~~improve the signal-to-noise ratio, we applied ~~each trace was~~ bandpass filter~~ed~~ up to 8 Hz and displayed the seismic section~~sed~~ ~~in reduced time~~ using a reduction velocity of 6 km s^{-1} ~~based on a velocity of 6 km/s in the breadth~~over a time window of -5–10 s (e.g. Fig. 2, Fig. 3).

Uncertainties in phase picking primarily arise from challenging signal-to-noise conditions and complex subsurface wave propagation effects. The extensive desert sedimentary cover in the study area significantly attenuates seismic energy, particularly at larger offsets and for deeper arrivals. Additionally, strong lateral heterogeneities, ~~—s~~such as fault zones and intracrustal velocity variation, ~~s—~~cause substantial wave scattering, dispersion, and multipathing. This~~,~~ result~~sing~~ in phase superposition and waveform distortion that complicates accurate phase identification. Following careful analysis and comparative evaluation, s~~S~~ix seismic phases, including Pg, P1, P2, P3, P4, Pm and Pn, are identified ~~based on the reduced seismic recordings~~ (e.g. Fig. 2, Fig. 3). Pg is a first-~~arriving~~ arrival phase refracting through ~~propagating over~~ the crystalline basement. Pm is the strongly wide-angle reflected phase from the Moho ~~discontinuity~~. Pn is the head wave refracted phase from the top of the mantle with a characteristic velocity of 7.7–8.~~0~~1 ~~km/s~~km s^{-1}. P2–P4 are the reflected phases from the intracrustal second-order velocity interfaces. In Fig. 2 and Fig. 3, the dotted lines represent the identified phases, and the squares mark the position of the computed traveltime.

The first-arrivals of Pg are picked up to offset of 100 km. ~~the~~ The travetimes recorded at ~~of~~shotpoint ZB1, located in the NQS, ~~are~~is early as are the ~~, which reveals the shallow velocity of the NQS is high with 5.1–6.3 km/skm s−1 and 4.0–6.1 km/skm s−1 average velocity correspondingly. The t~~traveltimes for the shot ZB8 located ~~of the north branch of ZB8 is early too, demonstrating the shallow crustal velocity~~ in the northern ~~Beishan block~~BOC ~~is with 3.3–6.3 km/skm s−1~~. Intracrustal reflection phases P2–P4 can be recognized at the offset ranges from 70–90 km, 100–150 km, and 120–150 km respectively. Pm can be corelated over an offset of 180 km for most shots (Fig. 4a). Pn was found with maximal amplitude in the offset range of 240–280 km (Fig. 3). ~~The Pn displayed in shot ZB1 seismic record is with 7.9–8.1 km/skm s−1 velocity, while 7–8.1 km in shot ZB8 (Fig. 4).~~

~~The~~ V~~v~~elocity ~~structure m~~Modelling

The ~~2-D crustal velocity structure is based on seismic phases identification, and the first~~ initial 2-D crustal model ~~is~~ was ~~built~~ constructed ~~with~~ using the ~~greatest~~ highest elevation of 4300 m as the datum. The f~~F~~~~The f~~orward fitting calculation adopts the asymptotic ray tracing to fit the traveltime of each shot (Fig. 4; ~~(~~Cervený~~y~~ et al. 1988; Vidale 1988; Zelt and Smith 1992; Cervený 2001) and gradually improves the initial 2-D velocity structure by constantly modifying the interface depth and interval velocity. Model construction and editing are carried out with the RAYINVR software (Zelt and Smith, 1992). The travetime fitting of 5–6 phases for nine shots are conducted step by step, top-down to limit the multi-solution of the model. Fig. 4 illustrates the traveltime fitting of the seismic recordings of the shot gather and the complete crustal ray coverage. The time error of the ray tracing forward fitting accuracy is typically less than 0.05 s, and the maximum is not more than 0.1 s. The root mean square error (RMS) of the traveltime fitting for different earthquake phases is reported in Table 2. The velocity inaccuracy is controlled within 0.05 ~~km/s~~km s^{-1}, while the Moho depth error is less than 1 km. The ultimate crustal-upper mantle velocity structure is found in Fig. 5. The typical continental crust is stratified into three principal layers: the upper crust, comprising sedimentary cover overlying crystalline basement characterized by an average P-wave velocity of 6.0–6.3 km s^{-1}; the mid~~dle~~ crust, composed of interleaved silicic and basic lithologies, with velocities of 6.3–6.5 km s^{-1}; and the lower crust, dominated by more mafic assemblages, exhibiting velocities of 6.6–6.9 km s^{-1} (Christensen, 1995; Jia et al., 2019). Based on our velocity structure result, ~~The result shows~~ the crust can be ~~split~~divided into upper crust (from the surface to ~~P2~~C2), middle crust (from ~~P2~~ C2 to ~~P3~~C3), and lower crust (from ~~P3~~ C3 to the Moho ~~discontinuity~~). The upper crust can be separated into two layers by intracrustal interface C1 determined by seismic

设置了格式: 上标

设置了格式: 上标

设置了格式: 上标

phase P2. The lower crust can also be subdivided~~separated~~ into two layers~~strata as well as~~ by intracrustal interface C4 indicated by seismic phase P4.

Velocity S~~s~~tructure of the U~~u~~pper Crust

The upper crust, from~~comprising delineated by~~~~the layer from~~ the surface to interface C2 at depth, ~~has pronounced~~exhibits pronounced lateral segmentation across the study region. Lower velocities extend to greater depth ~~Notably, A prominent~~~~a lower- velocity zone is prevalent~~ beneath~~in~~ the NQS~~orth Qilian~~-Jiuquan basin, contrasting sharply laterally with the ~~a~~ significantly ~~greater~~ higher velocities characteristic of~~y zone in~~ the ~~Beishan block~~BOC. Along interface C1 ~~amid~~ within the upper crust, discrete~~many~~ high-velocity ~~entities~~ zones with ~~an~~ interval velocities~~y~~ of 6.3–6.4 ~~km/s~~km s^{-1} are ~~seen~~observed.

~~The base of i~~Interface C1 ~~corresponds to~~marks the basement surface, characterized by ~~a~~ velocities~~y~~ ranging~~e~~ from~~e~~ ~~of~~ 3.4 to –6.5 ~~km/s~~km s^{-1}. The basement ~~profile~~ surface exhibits significant undulations~~es extensively~~ within~~in the~~ depths varying between~~of~~ 6.1 and –12.5 km (Fig~~. 5b~~. 5). The interval velocity of the uppermost crust ~~measures~~ ranges from 5.2 to –6.05 ~~km/s~~km s^{-1}, with an interface depth of 6.3–7.2 km in the ~~middle~~ central ~~Qilian~~NQS. In the southern ~~North Qilian~~NQS, the interval velocity ~~ranges from~~is between 5.2 and –6.1 ~~km/s~~km s^{-1}, ~~having~~ and a high-velocity ~~body~~zone is present in the ~~bottom~~ lower section, with ~~an~~ interval velocities~~y~~ of 6.2–6.45 ~~km/s~~km s^{-1}~~,~~; here, the ~~and the~~ interface de~~e~~pens~~th lowers~~ to 10.8–11.4 km. In the northern ~~section of the North Qilian~~NQS, the interval velocity ~~falls~~ decreases to 4.0–6.0 ~~km/s~~km s^{-1}, while the interface depth ~~deepens~~ increases to 9.7–10.1 km.

Within~~In~~ the Jiuquan basin, the interval velocity ~~reduces~~ ranges from~~to~~ 3.6 to –6.1 ~~km/s~~km s^{-1}, ~~with an~~and the interface de~~e~~pens~~pth falling~~ to 11.2–12.5 km. The Huahai basin ~~has~~ shows~~an~~ interval ~~velocity~~ velocities of 3.8–6.2 ~~km/s~~km s^{-1}, ~~and the~~with interface depths between ~~ranges from~~ 11.5 and –12.5 km. A~~dditionally, a~~ high-velocity ~~body~~ zone with ~~an~~ interval ~~velocity~~ velocities of 6.3–6.5 ~~km/s~~km s^{-1} ~~appears~~ is also observed beneath ~~at the bottom below~~ the F5 fault~~racture~~. In the southern ~~Beishan block~~BOC, ~~layer~~interval velocities on the south side ~~measure~~ are 4.6–6.2 ~~km/s~~km s^{-1}, with interface depths ~~ranging from~~of 11.5–12.0 km, whereas on the northern side, ~~layer~~interval velocities ~~reduce~~ decrease to 3.4–6.1 ~~km/s~~km s^{-1}, and interface depths ~~are~~ range from 9.4 to– 11.3 km.

In the Northern ~~Beishan block~~BOC, ~~layer~~interval velocities ~~are~~ vary from 4.2 to –6.2 ~~km/s~~km s^{-1}, with the~~an~~ interface at depths of 10.5–12.5 km. Further north within the ~~Beishan block~~BOC, the interval velocity ~~is~~ remains between 4.2 and –6.2 ~~km/s~~km s^{-1}, and the interface depth ~~is~~ ranges from 10.0 to –11.3 km. ~~At the bottom of the Beishan blockBOC, multiple~~ Several high-velocity ~~bodies~~zones ~~are observed~~ with ~~layer~~interval velocities of 6.3–6.4 ~~km/s~~km s^{-1} are identified at the base of the BOC, including one beneath ~~the high-velocity body under~~ the ~~Mazhoushan~~ Mazongshan ~~terrane~~arc.

The deeper upper crustal~~bottom~~ layer exhibits velocities ~~ranging from~~of 6.0–6.3 ~~km/s~~km s^{-1} and interface depths ~~ranging from~~between 13.2 and –27.6 km. Although this layer shows no ~~While lacking significant~~major lateral segmentation, its interface is highly undulatory~~this layer exhibits considerable interface undulations~~ (Fig~~. 5b~~. 5). South of fault F9, the interval velocity is 6.05–6.15 ~~km/s~~km s^{-1}, with ~~an~~ the interface ~~depth of~~ at 12.8–18.3 km depth. Between faults F9 and F5, the layer thickens ~~substantially~~considerably, and the interface ~~depth climbs~~deepens to 17.6–27.5 km. North of fault F5, the layer thickness ~~reduces~~ decreases to values similar to those in~~match~~ the southernmost part of the profile, but the velocity increases to 6.1–6.4 ~~km/s~~km s^{-1}. ~~This~~ These characteristics ~~shows~~ indicate that the ~~North Qilian~~NQS –and the Jiuquan basin ~~have~~ share a consistent basement structure, ~~matching~~ which aligns with the findings from residual gravity anomaly ~~findings~~analyses (Yang et al. 2024).

V~~v~~elocity S~~s~~tructure of the M~~m~~id-~~dle~~ C~~e~~rust

The intermediate crust –exhibits distinct zoning features ~~of the intermediate crust are notably~~that differ ~~notbly~~notably~~ent~~ from the ~~top~~ upper crust with~~,~~ ~~with interface depth of 23.4–38.7 km,~~ and~~d~~ ~~layer~~ interval velocity~~ies~~ of 6.2–6.5 ~~km/s~~km s^{-1}. This layer is ~~There're c~~Comparatively slower~~ly low-velocity zones are observed~~ ~~occurring in~~beneath the northern ~~North Qilian~~NQS and

设置了格式: 字体: (中文) +中文标题 (等线 Light), 10.5 磅, 加粗
设置了格式: 字体: (中文) +中文标题 (等线 Light), 10.5 磅, 加粗
设置了格式: 上标
设置了格式: 上标
设置了格式: 上标
设置了格式: 上标
设置了格式: 上标
设置了格式: 上标
设置了格式: 上标
设置了格式: 上标
设置了格式: 上标
设置了格式: 上标
设置了格式: 上标
设置了格式: 上标
设置了格式: 上标
设置了格式: 上标
设置了格式: 上标
设置了格式: 上标
设置了格式: 上标

the Jiuquan basin (Fig. 5).

The interface C3 depth across the fault F8 separating the NQS and the Jiuquan basin varies from 23.4 to 38.7 km. The lowest interval velocities (6.2–6.35 km s^{-1}) occur in the central NQS, increasing northward to 6.25–6.45 km s^{-1}. In the Huahai basin, the interface lies at 27.5–38.7 km depth, with interval velocities of 6.25–6.5 km s^{-1}; the highest interval velocity in this region (6.32–6.45 km s^{-1}) are found in its central part (Fig. 5).

Within the BOC, the interface C3 shallows to 24.4–31.2 km. Mid-crustal interval velocities in the Shibanshan arc are 6.3–6.5 km s^{-1}, decrease to 6.25–6.4 km s^{-1} in the southern Shuangyingshan arc, and increase to 6.3–6.42 km s^{-1} further north.

The velocity contours display contrasting dip directions: in the NQS and the Jiuquan basin, they show a gently undulating northward inclination, while in the Huahai basin they dip steeply southward (Fig. 5).

Velocity Structure of the Lower Crust

The lower crust can be subdivided into three segments from south to north, bounded by faults F9 and F4 (Fig. 5). The consistent undulation of the interface C4 and Moho signifies the thickness variations of the upper and lower portions of the lower crust follow a similar trend along the entire profile.

Upper layer: This layer between C3 and C4 has an interval velocity of 6.45–6.7 km s^{-1} (Fig. 5). South of fault F9, interface C4 lies at depths of 36.7–42.4 km, with interval velocity of 6.45–6.7 km s^{-1}. Between faults F9 and F4, interface C4 deepens to 38.6–49.2 km, and the interval velocity increases to 6.5–6.7 km s^{-1}. Notably, a significant upward undulation of a high-velocity zone is observed in this segment. North of the fault F4, interface C4 shallow to 37.4–40.3 km, accompanied by a decrease in interval velocity to 6.47–6.65 km s^{-1}.

Lower layer: The Moho is identified at depths of 47.5–60.0 km and this layer between C4 and the Moho exhibits an interval velocity of 6.65–6.85 km s^{-1} (Fig. 5). Beneath the Qilian Shan and Jiuquan basin, the Moho reaches depth of 57.8–60.0 km, with an interval velocity of 6.7–6.85 km s^{-1}. The central Jiuquan basin exhibits the deepest Moho (60 km), where the interval velocity decreases slightly to 6.7–6.78 km s^{-1}. In the Huahai basin and the BOC, the Moho depths range from 47.5 to 57 km, and the velocities reduces to 6.7–6.75 km s^{-1}. The shallowest Moho (at 47.5 km) is observed beneath the Que'ershan arc, where the lowermost crust has an interval velocity of 6.65–6.78 km s^{-1}.

Mantle velocity structure revealed from Pn

The mantle velocity structure exhibits distinct lateral variations across the study area. The Qilian Shan is characterized by a relatively high uppermost mantle velocity range of 7.9–8.3 km s^{-1}, with sub-horizontal velocity contours. A velocity reduction to 7.7–8.3 km s^{-1} is observed from the Jiuquan basin to the Shibanshan arc, followed by a slight increase to 7.9–8.3 km s^{-1} beneath the Shuangyingshan arc. Further north, the Mazongshan, Hanshan, and Que'ershan arcs show progressively lower Pn velocities, ranging from 7.8 to 8.2 km s^{-1}, indicating a south-to-north decreasing trend. The lowest Pn values (7.7–7.8 km s^{-1}) are localized beneath faults F5, F1, and F6.

~~**Crustal Velocity Structure Implications**~~

~~The crustal velocity structure proposes an unusual scenario where the deepest Moho is found in the central Jiuquan basin, rather than the North Qilian Shan with the highest elevation. Additionally, the Qilian Shan and southern Shibanshan terrane exhibit a thin upper-middle crust and a thick lower crust, while other parts have the reverse pattern (Fig. 5b. 5)~~

Crustal-U~~u~~pper M~~m~~antle V~~v~~elocity A~~a~~nomaly S~~s~~tructure

To improve the visibility~~sensitivity~~ of the velocity heterogeneity of the crustal-upper mantle structure the mean layer velocities are subtracted to produce a velocity anomaly structure of the crustal-upper mantle ~~is determined~~ (Fig~~. 6b~~. 6~~, the difference between the velocity contour values and their mean values). Figu~~). Figure 6b demonstrates that in the upper layer of the crust from depths of 0 to 12.5 km, the composition is significantly heterogeneous, and lateral segmentation is visible. The Qilian Shan is with a high positive velocity anomaly (0.3–1.0 ~~km/s~~km s^{-1}). The Jiuquan basin and Huahai basin show~~are with~~ negative velocity anomaly (-1.1– -0.15 ~~km/s~~km s^{-1}), and extend northward to the southern Shuangyingshan ~~terrane~~arc, which ~~are prevented~~terminate at~~by~~ the strong positive velocity anomaly in the central Shuangyingshan ~~terrane~~arc. Three positive velocity anomaly bodies (0.12–0.45 ~~km/s~~km s^{-1}) with closed contours exist beneath the faults F5, F4, and the core Shuangyingshan ~~terrane~~arc. In the northern Shuangyingshan ~~terrane~~arc, a negative velocity anomaly (-1.3–-0.12 ~~km/s~~km s^{-1}) develops, and thins out to the north extending to the southern Mazongshan ~~terrane~~arc. The positive velocity anomaly (0.15–0.45 ~~km/s~~km s^{-1}) starting from the Mazongshan ~~terrane~~arc ~~dives~~ extends northward to the northern end of the Que'ershan ~~terrane~~arc, and the central part is covered by the low-velocity negative anomalies (-0.4–-0.08 ~~km/s~~km s^{-1}) in the upper Hanshan ~~terrane~~arc.

At a depth of 9.2–38.5 km between interface C1 and C3, the middle Qilian and the southern ~~North Qilian~~NQS consisted of the northward-tilted, small-variation positive velocity anomalies (0.0 to 0.08 ~~km/s~~km s^{-1}) and negative anomalies (-0.03–-0.01 ~~km/s~~km s−1). The northern ~~North Qilian~~NQS, the Jiuquan basin and the southern portion of the Huahai basin are northward-tilted, downward-curved layers of the low-velocity negative anomalies (-0.05–-0.2 ~~km/s~~km s^{-1}). The northern half of the Huahai basin and the Shibanshan ~~terrane~~arc are positive anomaly (0.0–0.08 ~~km/s~~km s^{-1}) layers with small velocity changes. The southern Shuangyingshan ~~terrane~~arc is a mixed layer of the positive velocity anomaly (0.01–0.08 ~~km/s~~km s−1) and negative velocity anomaly (-0.01–-0.04 ~~km/s~~km s^{-1}). The velocity anomaly from the northern Shuangyingshan ~~terrane~~arc to the Que'ershan ~~terrane~~arc is positive (0.03–0.12 ~~km/s~~km s^{-1}), and only locally negative (-0.01–-0.03 ~~km/s~~km s^{-1}).

In the upper layer of the lower crust, the Qilian Shan is characterized by a positive velocity anomaly (0.01-0.12 ~~km/s~~km s^{-1}) in the upper section, and a negative velocity anomaly (-0.01-0.08 ~~km/s~~km s^{-1}) in the lower part. The Jiuquan basin and Huahai basin are characterized by minor negative velocity anomalies (-0.02–-0.08 ~~km/s~~km s^{-1}). The ~~Beishan block~~BOC is characterized by a strong positive velocity anomaly (0.02-0.12 ~~km/s~~km s^{-1}) and exhibits a northward-increasing trend (Fig~~. 6b~~. 6).

In the lowest layer of the lower curst, From the ~~North Qilian~~NQS to the southern Huahai basin, the velocity anomaly reveals positive (0.01-0.07 ~~km/s~~km s^{-1}) with a relatively minor variance. From the northern Huahai basin to the southern Shuangyingshan ~~terrane~~arc, the velocity anomaly is with a positive to negative (0.01–-0.07 ~~km/s~~km s^{-1}) from top to bottom. From the northern Shuangyingshan to the Que'ershan ~~terrane~~arc, lesser positive anomalies (0.01 to 0.03 ~~km/s~~km s^{-1}) are observed (Fig~~. 6b~~. 6).

At the top of the upper mantle, the ~~North Qilian Shan~~NQS and the southern Jiuquan basin show positive velocity anomaly with modest changes (0.05-0.15 ~~km/s~~km s^{-1}), whereas negative anomaly with substantial velocity variations (-0.1 to -0.25 ~~km/s~~km s^{-1}) from the northern Jiuquan basin to the Shibanshan ~~terrane~~arc. The southern Shuangyingshan ~~terrane~~arc is characterized with a gradient of the velocity anomaly ranging from negative to positive (-0.1–0.12 ~~km/s~~km s^{-1}). The northern Shuangyingshan and Mazongshan display positive anomaly (0.03–0.12 ~~km/s~~km s^{-1}) moving downwardly. The southern Hanshan ~~terrane~~arc has a positive anomaly (0.01–0.1 km s^{-1}) characterized by a gradual reduction from south to north. The northern Hanshan ~~terrane~~arc and the

Que'ershan ~~terrane~~arc show negative anomaly (-0.01–-0.12~~-~~ km s^{-1}) that diminish steadily from south to north (Fig~~. 6b~~. 6).

Discussion

The ~~observed~~ crustal-upper mantle structure (Fig. 5; Fig. 6) records~~is~~ a what is know to be a complicated ~~outcome~~ history ~~shaped by both~~ of vertical and lateral ~~material~~ mass transfer~~port processes~~, reflecting Precambrian inheritance~~re.~~. ~~These activities are related to~~ Paleozoic subduction~~, collision, and~~ /accretion ~~events~~, Mesozoic intracontinental ~~deformations~~reworking, and ~~the~~ Cenozoic northward ~~spread~~ expansion of the NE ~~Tibetan~~ Tibetan plateau (Cunningham et al., 2009; Zhang and Cunningham, 2012; Li et al., 2021~~REFERENCES~~)~~since the Precambrian~~.

The N~~n~~ature of the Beishan Orogenic Collage ~~BOC~~ crust

It has been previously interpreted that ~~T~~the mid~~dle~~-lower crust beneath the BOC behaves as a mechanically stable 'fossil archive' on Cenozoic time scales, preserving pre-Cenozoic architecture, whereas the~~–~~ uppermost mantle and upper crust show active deformation (Cui et al. 1995). Instrumentally recorded seismicity is~~n~~ confined to the Qilian Shan, the Hexi Corridor basins, the Huahai Basin, and local areas west of Xingxingxia, mostly at depths ~~of~~above? 15–16 km (Fig. 7),), which acted as the decollement as shown in the seismic profile (Fig. 5, Fig.6; Fig. 8)~~.~~. T~~t~~he Beishan interior has spatially and temporally sparse low magnitude~~is almost aseismic~~ (M< 4.7) seismicity and exhibits low topographic relief (Xiong et al. 2003; Yang et al. 2019; Zhao et al. 2019), indicating limited present-day strain. Slight mid-lower-crustal flexure and reduced resistivity in southern Beishan (Xiao et al. 2015) nevertheless imply a rheologically (not seismically) slightly weaker zone relative to its surroundings. Active left-lateral and thrust faults in the southern BOC also indicate a weaker crust (Yang et al. 2019; Zhang et al. 2020; Yun et al. 2021; Zhang et al. 2023).

Paleozoic ~~Subduction~~ S~~s~~ubduction P~~p~~olarity ~~of the Qilian Ocean and the southern PAO~~and A~~a~~ccretionary A~~a~~rchitecture

Strata of

~~T~~the ~~North~~ Qilian Ocean, a ~~part~~ branch of the Proto-Tethys Ocean, deforms~~evolved predominantly~~ along the Kunlun, ~~Mts.,~~ Qilian ~~Shan and~~, Altyn mountain belt~~Mts.~~ in the northern ~~Tibetan Plateau~~Tibetan Plateau. The dynamics of the closure of the Qilian Ocean ~~resulting from the collision~~via collision between the ~~Kunlun-~~Qaidam continent and the southern ~~boundary~~ margin of the North China Craton remains ~~a matter of considerable~~ debated (Yin and Harrison 2000; Guterch et al. 2003; Xiao et al. 2009; Song et al. 2014; Wu et al. 2017; Zuza et al. 2017; 2019). The subduction polarity of ~~this~~ the ~~ocean~~Qilian Ocean has been proposed as: 1) north-dipping (Zuo and Liu 1987; Song et al. 2013; Li et al. 2022); 2) south-dipping (Wang and Liu 1981; Li et al. 2016); 3) bidirectional (Zhao et al. 2024); ~~or~~ or divergent models (Wu et al. 2011; Chen et al. 2019). Although previous geophysical investigations have covered the Qilian Shan (Xiao et al. 2016; Guo et al. 2019; Shen et al. 2020; Li et al. 2021), focus~~concentration~~ has largely been on neotectonics rather than Paleozoic evolution. In this study, we observed north-dipping velocity contour from interface C2 to the uppermost mantle beneath the Qilian Shan, coupled with a lower-crust–upper-mantle low velocity anomaly beneath the Hexi Corridor (Fig. 6). These features most plausibly record early Paleozoic north-dipping subduction of the Qilian Ocean, which aligns with the surface geology; later collisional or bidirectional shortening may have locally overprinted the original polarity (Davis and Darby, 2010).

Despite intensive geochemical and chronological research on Paleozoic rocks in the Dunhuang block and the BOC, the accretionary architecture of the PAO ~~still remains~~remained enigmatic (Xiao et al. 2010; Shi et al. 2020, 2021; Li et al. 2023). Our deep seismic velocity model now provides the direct geophysical evidence for the subduction polarity within the northern BOC. Beneath the Que'ershan arc, the northernmost portion of the BOC, north-dipping velocity contours from interface C2 to the Moho imply south-dipping subduction of the Hongshishan Ocean, consistent with surface geology (Xiao et al. 2018; Duan et al. 2020; Niu et al. 2020; Xin et al. 2020). Velocity undulations between faults F9 and F1 probably reflect late-Paleozoic collision or Cenozoic bidirectional compression, obscuring primary dip direction.

设置了格式: 上标

设置了格式: 俄语

带格式的: 标题 2

带格式的: 正文

设置了格式: 字体颜色: 自动设置

设置了格式: 字体颜色: 自动设置

设置了格式: 字体颜色: 自动设置

设置了格式: 字体颜色: 自动设置

设置了格式: 字体颜色: 自动设置

设置了格式: 字体颜色: 自动设置

设置了格式: 字体颜色: 自动设置

设置了格式: 字体颜色: 自动设置

Between faults F2 and F4, a positive upper-mantle velocity anomaly (8.0–8.3 km s^{-1}) between ~45 km and ~70 km depth likely represents a broken off fossil ~~breakoff~~ subduction slab following north-dipping subduction of the Beishan Ocean, although residual oceanic crust or mafic underplating cannot be entirely excluded. This anomaly aligns with the Hongliuhe–Xichangjing ophiolite mélange in surface (Yu et al. 2012; Hu et al. 2015; Song et al. 2015; Wang et al. 2015; Li et al. 2023).

Cenozoic C~~cC~~rustal D~~d~~eformation and S~~s~~train P~~p~~artitioning across M~~m~~ajor F~~f~~aults~~mechanism~~

Northward-propagating crustal shortening since the Miocene is accommodated through a series of parallel NW-SE-trending thrust faults in the Qilian Shan and successively reaches the Hexi corridor and the BOC (Cunningham 2010, 2013; Wang et al., 2020; Yu et al., 2021; Zhang et al. 2023).

Symmetric downward undulation of the velocity contours (6.2–6.8 km s^{-1}) across the southern margin fault of the Beishan (F5) demonstrates that fault F5 acts as a lithospheric-scale partition zone rather than other faults (Fig. 5, Fig. 6). South of the fault F5, north-tilting high velocity anomaly bodies with 6.2–6.45 km s−1 at the base of the upper crust (18–25 km depth) form the Qilian Shan to the Shibanshan arc, correlate to the north-vergent thrusting that decouples from a co-thickened middle-lower crust (25–50 km, 6.5–6.8 km s^{-1}). North of the fault F5, complementary velocity gradients (6.1–6.6 km s^{-1}, 15–45 km) indicate conjugate north-direction upper-crustal thrusting accompanied by whole-crust gentle folding in the BOC. The downward-undulation of the velocity contours imply co-thickening of the middle-lower curst of the NQS–Shuangyingshan area, with the uppermost crust experiencing thrusting and overthrusting. Our velocity structure indicated that low Pn velocity with 7.7–7.9 km s^{-1} and dome-shaped uplift of the crust directly beneath the fault F5 (Fig. 5). The electrical resistivity imaging (Yang et al. 2019) also highlighted the boundary fault, termed Baihewan fault (in Fig. 7) in the southernmost Shibanshan arc; ~~,~~ this fault~~which~~ penetrates the lower crust with low resistivity, to both sides of which the direction of the interpreted thrusting is opposing ~~(Yang et al. 2019)~~.

The s~~S~~eismic reflection profile revealed a south-dipping Cenozoic thrusting system that dislocated the Paleozoic–Mesozoic strata over the undeformed Meso-Cenozoic sediments in the Jiuquan basin (Zuza et al. 2016; Huang et al. 2021), consistent with our velocity model. The shallow velocity structure across the Huahai basin and the southern BOC likewise depicted the differences to both sides of F5 (Wu et al. 2022). Guo et al. (2019) likewise documented the northward expansion of the Qilian Shan across the Hexi corridor via uppermost-crustal overthrusting and lower-crustal thickening east of our seismic profile. High-resolution seismic reflection profile south of the fault F5 further reveals the middle-lower crustal thickening by duplexing (Huang et al. 2021).

Within the southern BOC north of the fault F5, north-direction thrusting dominates the uppermost crust, while the rest of crust undergoes gentle folding identical to the NQS–Hexi corridor style (Gaudemer et al. 1995; Meyer et al. 1998; Tapponnier et al. 2001; Yuan et al. 2013; Zuza et al. 2017; 2019). Crustal deformation across the fault F5 is therefore distinctly asymmetric: south of the fault, the uppermost crust is decoupled from the underlying crust (Fig. 5), whereas north of the fault the entire crust participates in coherent gentle folding (Fig. 8).

~~While past geophysical investigations have covered the Qilian Shan (Xiao et al. 2016; Guo et al. 2019; Shen et al. 2020; Li et al. 2021), concentration has largely been on neotectonics rather than Paleozoic evolution.~~

设置了格式: 检查拼写和语法
设置了格式: 检查拼写和语法
设置了格式: 字体: 非倾斜, 检查拼写和语法
设置了格式: 检查拼写和语法
设置了格式: 检查拼写和语法
设置了格式: 检查拼写和语法
设置了格式: 字体: 非倾斜, 检查拼写和语法
设置了格式: 检查拼写和语法
设置了格式: 检查拼写和语法
设置了格式: 检查拼写和语法
设置了格式: 字体: 非倾斜, 检查拼写和语法
设置了格式: 检查拼写和语法
设置了格式: 检查拼写和语法
设置了格式: 检查拼写和语法
设置了格式: 字体: 非倾斜, 检查拼写和语法
设置了格式: 检查拼写和语法
设置了格式: 检查拼写和语法
设置了格式: 上标
设置了格式: 非突出显示
设置了格式: 非突出显示
设置了格式: 非突出显示

Our data demonstrates a northward-tilted velocity contour from interface C2 to the topmost mantle beneath the Qilian Shan (Fig. 5b). This inclination suggests the northward descent of the middle crust to the uppermost mantle beneath the Hexi corridor. We speculate that this trait reflects a north-dipping subduction polarity of the Qilian Ocean in the early Paleozoic. Further corroborating our thought is the negative velocity anomaly body spanning from the lower crust to the topmost mantle beneath the Hexi corridor and southern Shibanshan (Fig. 6b).

带格式的: 标题 2

The Central Asian Orogenic Belt (CAOB) is well acknowledged for its southward migration throughout development and composition from 1000 Ma to 250 Ma (Lehmann and al. 2010; Jian et al. 2014; Kröner et al. 2014; Xiao et al. 2018). Consequently, the Dunhuang block, positioned at the southernmost extent of the CAOB and associated with the Beishan block, assumes a vital role in unraveling the decisive closure of the southern Paleo-Asian Ocean (PAO). Despite detailed geochemical and chronological research on Paleozoic rocks in the Dunhuang block and the Beishan block, the amalgamation style of the PAO remains elusive (Xiao et al. 2010; Shi et al. 2020, 2021; Li et al. 2023).

The previous Golmud–Ejin seismic profile defined the crustal structure of the Beishan block into three strata with an active upper mantle and stable crust (Cui et al. 1995), consistent with our current profile. The stable crust, specifically the middle-lower crust, is crucial in conserving fossil architecture. The north-tilted velocity contour beneath the Que'ershan terrane from interface C2 to the Moho discontinuity implies the crust north of the Que'ershan subducted beneath the Hanshan terrane, a deduction supported by geological observations (Xiao et al. 2018; Duan et al. 2020; Niu et al. 2020; Xin et al. 2020). Consequently, we suggest the subduction polarity of the Hongshishan Ocean as south-direction. The zone between F9 and F1 faults reveals a peculiar undulation of velocity profiles, presumably caused by subsequent late Paleozoic collision or bidirectional compression in the Cenozoic, complicating the distinction of subduction direction. Combining geological findings (Yu et al. 2012; Hu et al. 2015; Song et al. 2015; Wang et al. 2015), we propose that the positive velocity anomaly body in the upper mantle between faults F2 and F4 could represent the fossil breakoff subduction slab following the north-dipping subduction of the Beishan Ocean, marked by the Hongliuhe–Xichangjing ophiolite mélange (Li et al. 2023).

Crustal deformation mechanism

Situated between the Tibetan Plateau and Mongolian plateau, the crust from the Qilian Shan to the Beishan block has undergone intracontinental deformation to varied degrees (Cunningham 2010, 2013; Zhang et al. 2023). The Qilian Shan, regarded as the youngest uplifted Mts. of the Tibetan plateau, absorbs significant shortening strain (Gaudemer et al. 1995; Meyer et al. 1998; Gao et al. 2013; Zuza et al. 2017), by a series of parallel NW-SE-trending thrust faults (Meyer et al. 1998; Tapponnier et al. 2001; Yuan et al. 2013; Zuza et al. 2017). Progressive deformation commenced in Miocene, extending northward to the Hexi corridor and Beishan–Alxa block (Wang et al. 2020; Yu et al. 2021; Zhang et al. 2023). The seismic profiles (Fig. 5b, Fig. 6b) reveal two distinct downward-undulation velocity contours on either side of the southern boundary fault of the Beishan (F5). This suggests F5 as the boundary fault restricting compressional stress from the north and south.

带格式的: 标题 2

In the area south of F5, northward-tilted positive velocity anomaly bodies with 6.2–6.45 km/s velocity at the base of the upper crust form the Qilian Shan to the Shibanshan terrane, correlate to the north-direction thrust faults. In the area north of F5, the opposite velocity features imply north-direction thrusting in the upper crust of the Beishan block. The downward-undulation of the velocity contours imply co-thickening of the middle-lower curst of the NQS–Shuangyingshan area, with the upper crust experiencing thrusting and overthrusting. Our velocity structure indicated that low Pn velocity with 7.7–7.9 km/s and dome-shaped uplift of the crust directly beneath F5 (Fig. 5b). The electrical resistivity imaging also highlighted the boundary fault, termed Baihewan fault (BHWF in Fig. 7) in the southernmost Shibanshan terrane, which penetrates the lower crust with low resistivity, to both sides of which the direction of the thrusting is opposing (Yang et al. 2019). The shallow velocity structure across the Huahai basin and the southern Beishan block likewise depicted the differences to both sides of F5(Wu et al. 2022), which is aligned with our result (Wu et al. 2022). Collectively, we suggest F5 is a large-scale strike-slip fault which restricts the stress transmission further to both sides.Eastern Eextension of the Altyn Tagh FaultATF

The ~1600 km-long ATF is a major left-lateral strike-slip fault that defines the northern boundary of the Tibetan Plateau (Yin et al., 2002; Ritts et al., 2004; Dai et al., 2023; Xie et al., 2024). While its western and central segments are well-defined (Xie et al., 2023; Wu et al., 2024; Yao et al., 2025), its eastern termination and continuation remain highly controversial due to extensive sedimentary cover of the desert and discontinuous bedrock outcrops (Yue et al., 2001; Cunningham and Zhang, 2020; Yang et al., 2023). Definition of its eastern extentThe resolution of this debate is critical for understanding deformation propagation into northeast Tibetan plateau and for regional seismic hazard assessment. Yue et al. (2001) proposed that the ATF likely extends east-northeast to northeast along the Alxa–East Mongolia fault (Donskaya et al., 2008), with Cenozoic motion displacing the Hexi Corridor and cutting through the BOC. An alternative view suggests that the ATF transfers its slip northward into the thrust systems along the northern margin of the Hexi Corridor, transitioning from predominantly strike-slip in the west to dip-slip in the east, where it eventually terminates against reverse faults within the Alxa Block (Xiao et al., 2015; Yang et al., 2023).

This study suggests that interprets F5 as the principal eastern splay of the ATF, the ATF does not terminate at the Qilian Shan frontland, but rather extendscontinues eastward to east-northeast into the BOC and the Alxa Block. The notable velocity contrast observed across the fault F5 may indicate the ATF extends at least across the southern margin of the BOC. -The projected left slip rate with of 1.52–2.69 mm/a, is significantlysubstantially greater higher than the thrust rate with of 0.35 mm/a in the southernmost Beishan area (Yang et al. 2019; Yun et al. 2021). Geodetic The GPS motion and velocities (Yang et al. y rate result fields revealed thats the moving direction changed from northeast in the Qilian Shan to nearly-east in the Beishan blockBOC with a significant lateral motion rates (Fig. 7; Yang et al., 2021). Darby et al. (2005) identified five major left -lateral strike-slip faults within the BOC and the Alxa block, which strike is consistent with the ATF, and accommodated ≥70 km post-Cretaceous offset based on Landsat/ASTER imagery and field mappingwork. Thus, we propose that the ATF continues straight eastward along a consistent NEE strike at the southern margin of the BOC.; Local faults identified within the southern margin of the BOC, such as the Beihewan fault, the Heishan fault, the Jiujing-Bantan fault, and the Ebomiao fault may be the secondary splays of the ATF and eventually terminate against it (Fig. 7; Yun et al., 2019; Zhang et al., 2020; Yang et al., 2019; 2024). These subsidiary structures collectively accommodate distributed crustal deformation These results further lend support to our result. Thus, theregionally. This kinematic model also provides a coherent explanation for the distinct slip-rate decline from the western-central to eastern segment of the ATF (Yan et al., 2024). Furthermore, the distribution of seismicity supports this structural boundary: all recorded earthquakes of M ≥ 4.57 occur south of the ATF and its eastern prolongation, with no events detected north of the fault within the interior of the BOC (Fig. 7). crustal deformation in this transition zone is different in the areas to both sides of F5. In the area south of F5, the upper and middle-lower crust is decoupled, and the deformation mechanism in the upper crust in north direction thrusting, and co-thickened in the middle-lower crust (Fig. 8).

The Seismic reflection profile revealed a south-dipping Cenozoic thrusting system that dislocated the Paleozoic–Mesozoic strata over the undeformed Meso-Cenozoic sediments in the Jiuquan basin (Zuza et al. 2016; Huang et al. 2021), which is compatible with our seismic imaging. Guo et al. (2019) also found the deformation and expansion of the Qilian Shan extended across the Hexi corridor by overthrusting in the top crust and thickening in the lower crust east to our study area. The seismic reflection profile over the southern segment of this section further supports the thickening mechanism of the middle-lower crust by duplexing (Huang et al. 2021). In the southern Beishan block north of F5, the north-direction thrust faults was playing the function in the top crust, and the middle-lower crust is folded alike the North Qilian–Hexi corridor area.

In NE Tibet and Beishan area, earthquakes predominantly occur in the Qilian Shan, Hexi Corridor basins, Huahai Basin, and local areas west of Liyuan, Hongliuhe, and Xingxingxia area, mostly at depths of 15–16 km (Fig. 7). The Beishan area is very stable, with few known earthquakes higher than magnitude 4.7 (Xiong et al. 2003; Yang et al. 2019; Zhao et al. 2019). The current low topographic relief also shows the Beishan block is relatively stable and tectonically inactive. However, our imaging suggests a slight bending of the middle-lower crust in the southern Beishan block, suggesting the middle-lower crust of the southern Beishan block is a little weaker than the bordering regions. Active left-lateral and thrust faults in the southern Beishan block support this assumption (Yang et al. 2019; Zhang et al. 2020; Yun et al. 2021; Zhang et al. 2023).

Conclusion

1). Crustal thickness decreases northward from 60 km beneath the central Jiuquan basin to 47.5 km beneath the Que'ershan arc; average crustal velocities (6.24 – 6.43 km s^{-1}) and uppermost mantlePn velocities (7.7 – 8.1 km s^{-1}) reveal strong lateral heterogeneity.

2). North-dipping velocity contours and a lower-crust – upper-mantle low-velocity corridor beneath the Hexi Basin support early Paleozoic north-dipping subduction of the Qilian Ocean; a positive upper-mantle anomaly (8.0 – 8.3 km s^{-1}, 45 – 70 km) between faults F2 and F4 represents a fossil break-off slab after north-dipping subduction of the Beishan Ocean.

3). Fault F5 acts as a lithospheric-scale partition: north-vergent, decoupled thrusting south of F5 versus whole-crust gentle folding to the north; a dome-shaped Moho and slow mantle Pn phase (7.7 – 7.9 km s^{-1}) beneath F5 localise present-day strain.

4). The Altyn Tagh Fault continues east-northeast along F5 into the Beishan and Alxa Block at 1.52 – 2.69 mm a^{-1} left slip, far exceeding the 0.35 mm a^{-1} thrust rate; secondary splays along the southern Beishan margin collectively accommodate deformation and explain the eastward slip-

设置了格式: 字体: (默认) Times New Roman, (中文) 宋体, 英语(美国)
带格式的: 段落间距段后: 0 磅, 无项目符号或编号, 字体对齐方式: 自动对齐, 图案: 清除
设置了格式: 字体: (默认) Times New Roman, (中文) 宋体, 英语(美国)
设置了格式: 字体: (默认) Times New Roman, (中文) 宋体, 英语(美国)
设置了格式: 字体: (默认) Times New Roman, (中文) 宋体, 英语(美国)
设置了格式: 字体: (默认) Times New Roman, (中文) 宋体, 英语(美国)
设置了格式: 字体: (默认) Times New Roman, (中文) 宋体, 英语(美国)
设置了格式: 字体: (默认) Times New Roman, (中文) 宋体, 英语(美国)
设置了格式: 字体: (默认) Times New Roman, (中文) 宋体, 英语(美国)
设置了格式: 字体: (默认) Times New Roman, (中文) 宋体, 英语(美国)
设置了格式: 字体: (默认) Times New Roman, (中文) 宋体, 英语(美国)
设置了格式: 字体: (默认) Times New Roman, (中文) 宋体, 英语(美国)
设置了格式: 字体: (默认) Times New Roman, (中文) 宋体, 英语(美国)
设置了格式: 字体: (默认) Times New Roman, (中文) 宋体, 英语(美国)
设置了格式: 字体: (默认) Times New Roman, (中文) 宋体, 英语(美国)
设置了格式 ...
设置了格式 ...
设置了格式 ...
设置了格式 ...
设置了格式 ...
设置了格式 ...
设置了格式 ...
设置了格式 ...
设置了格式 ...
设置了格式 ...
设置了格式 ...
设置了格式 ...
设置了格式 ...
设置了格式 ...
设置了格式 ...
设置了格式 ...
设置了格式 ...
设置了格式 ...
设置了格式 ...

rate decrease.

The crust thickness in the studied area spans from 47.5 to 60 km, separated into five strata. The thickest crust, measuring 58–60 km, spans from the Qilian Shan to the middle Jiuquan basin and gradually thins northward, with thicknesses of 55–58 km in the Dunhuang block, 51.5–55 km in the Shibanshan arc, and 47.5–51.5 km in the Shuangyingshan and Que'ershan terranes. Surprisingly, the deepest Moho (60 km deep) is found in the middle Jiuquan basin, not in the North Qilian Shan with the highest height. The average crustal velocity varies from 6.24 to 6.43 km/s, with crustal velocity fluctuations between 3.4 and 6.85 km/s. The velocity at the top of the upper mantle is observed at 7.7–8.1 km/s.

The study region is grouped into three parts based on present-day activity: the Qilian-Hexi corridor, the southern Beishan block, and the northern Beishan. The middle unit has softer crust compared to the others, and the deformation of the middle-lower crust in the southern Beishan block is considerably stronger than in the other two units.

(3) Subduction in the research area involves both north-direction and south-direction subduction of the Qilian Ocean and the Hongshishan Ocean.

(4) Bounded by F5 operating as a regional large-scale strike-slip fault, the crustal deformation process on both sides is similarly disconnected. In the Qilian-Hexi corridor, north-direction thrusting and overthrusting dominate, while in the Beishan block, south-direction thrusting and overthrusting rule. The middle-lower crust co-thickens throughout the entire research area.

Acknowledgments This work was jointly funded by the National natural Science Foundation of the China (Grant Nos. 42274134, 41774114, 42261144669), the Deep Earth Probe and Mineral Resources Exploration-National Science and Technology Major Project (2025ZD1007701), the China Geological Survey Project (Grant No. DD20230008, DD20179342 and DD20160083), and the China Scholarship Council.

References

Ao, S., Xiao, W. *et al.* 2016. Paleozoic accretionary orogenesis in the eastern Beishan orogen: Constraints from zircon U–Pb and 40Ar/39Ar geochronology. *Gondwana Research*, **30**, 224-235, https://doi.org/https://doi.org/10.1016/j.gr.2015.03.004

Ao, S.J., Xiao, W.J., Han, C.M., Mao, Q.G. and Zhang, J.E. 2010. Geochronology and geochemistry of Early Permian mafic–ultramafic complexes in the Beishan area, Xinjiang, NW China: Implications for late Paleozoic tectonic evolution of the southern Altaids. *Gondwana Research*, **18**, 466-478, https://doi.org/https://doi.org/10.1016/j.gr.2010.01.004

Ao, S.J., Guo, Q.Q. *et al.* 2012. Cambrian to early Silurian ophiolite and accretionary processes in the Beishan collage, NW China: implications for the architecture of the Southern Altaids. *Geological Magazine*, **149**, 606-625, https://doi.org/10.1017/S0016756811000884

BGMRGP. 1989. Regional Geology of Gansu Province. Geological Publishing House Beijing, China [in Chinese with English abstract].

Buslov, M.M. 2012. Geodynamic nature of the Baikal Rift Zone and its sedimentary filling in the Cretaceous–Cenozoic: the effect of the far-range impact of the Mongolo-Okhotsk and Indo-Eurasian collisions. *Russian Geology and Geophysics*, **53**, 955-962, https://doi.org/https://doi.org/10.1016/j.rgg.2012.07.010

Cerveny, P.F., Naeser, N.D., Zeitler, P.K., Naeser, C.W. and Johnson, N.M. 1988. History of Uplift and Relief of the Himalaya During the Past 18 Million Years: Evidence from Fission-Track Ages of Detrital Zircons from Sandstones of the Siwalik Group. *In*: Kleinspehn, K.L. and Paola, C. (eds) *New Perspectives in Basin Analysis*. Springer New York, New York, NY, 43-61, https://doi.org/10.1007/978-1-4612-3788-4_3

Cervený, V. 2001. *Seismic ray theory*. Cambridge university press Cambridge [in Chinese with English abstract].

Che, Z.C. and Sun, Y. 1996. The age of the Altun granulite facies complex and the basement of the Tarim basin. *Regional Geology of China*, **56**, 51-57 [in Chinese with English abstract].

Chen, X., Gao, R., Xiong, X., Shao, Z., Li, B. and Zhang, Y. 2019. Deep seismic reflection profiling and broad-band magnetotelluric sounding of the Qilian Orogenic Belt: evidence for bi-directional subduction of the Proto-Tethys Ocean plate and northward growth of the Qinghai-Tibet Plateau. *AGU Fall Meeting Abstracts*, T22C-03 [in Chinese with English abstract].

Cui, Z.-z., Li, Q.-s., Wu, C.-d., Yin, Z.-x. and Liu, H.-b. 1995. The crustal and deep structures in Golmud-Ejin Qi GGT. *Acta Geophysica Sinica*, **38**, 28-34 [in Chinese with English abstract].

Cunningham, D. 2010. Tectonic setting and structural evolution of the Late Cenozoic Gobi Altai orogen. *Geological Society, London, Special Publications*, **338**, 361-387, https://doi.org/https://doi.org/10.1144/SP338.17

Cunningham, D. 2013. Mountain building processes in intracontinental oblique deformation belts: Lessons from the Gobi Corridor, Central Asia. *Journal of Structural Geology*, **46**, 255-282, https://doi.org/https://doi.org/10.1016/j.jsg.2012.08.010

Cunningham, D., Davies, S. and McLean, D. 2009. Exhumation of a Cretaceous rift complex within a Late Cenozoic restraining bend, southern Mongolia: implications for the crustal evolution of the Gobi Altai region. *Journal of the Geological Society*, **166**, 321-333, https://doi.org/10.1144/0016-76492008-082

Dai, S., Fang, X., Chunhui, S., Junping, G., Donglin, G. and Jijun, L. 2005. Early tectonic uplift of the northern ~~Tibetan Plateau~~Tibetan Plateau. *Chinese Science Bulletin*, **50**, 1642-1652, https://doi.org/10.1360/03wd0255

Davis, G.A. and Darby, B.J. 2010. Early Cretaceous overprinting of the Mesozoic Daqing Shan fold-and-thrust belt by the Hohhot metamorphic core complex, Inner Mongolia, China. *Geoscience Frontiers*, **1**, 1-20, https://doi.org/https://doi.org/10.1016/j.gsf.2010.08.001

Donskaya, T.V., Windley, B.F. *et al.* 2008. Age and evolution of late Mesozoic metamorphic core complexes in southern Siberia and northern Mongolia. *Journal of the Geological Society*, **165**, 405-421, https://doi.org/10.1144/0016-76492006-162

Duan, L., Niu, W. *et al.* 2020. The petrogenesis of quartz diorite(350 Ma)from the Baiheshan area of the Beishan orogenic belt, and its chronological constraint on Hongshishan-Baiheshan Ocean's subduction initiation. *Geological Bulletin of China*, **39**, 1330-1340 [in Chinese with English abstract].

Gao, R., Hou, H. *et al.* 2013. Fine crustal structure beneath the junction of the southwest Tian Shan and Tarim Basin, NW China. *Lithosphere*, **5**, 382-392 [in Chinese with English abstract].

Gaudemer, Y., Tapponnier, P. *et al.* 1995. Partitioning of crustal slip between linked, active faults in the eastern Qilian Shan, and evidence for a major seismic gap, the 'Tianzhu gap', on the western Haiyuan Fault, Gansu (China). *Geophysical Journal International*, **120**, 599-645, https://doi.org/10.1111/j.1365-246X.1995.tb01842.x

Gehrels, G.E., Yin, A. and Wang, X.-F. 2003. Detrital-zircon geochronology of the northeastern ~~Tibetan plateau~~Tibetan Plateau. *GSA Bulletin*, **115**, 881-896, https://doi.org/10.1130/0016-7606(2003)115<0881:DGOTNT>2.0.CO;2

Guo, G., Wu, C. *et al.* 2019. Seismic anisotropy of the northeastern margin of the ~~Tibetan Plateau~~Tibetan Plateau derived from analysis of SKS and Pms seismic phases. *Chinese Journal of Geophysics*, **62**, 1650-1662 [in Chinese with English abstract].

Guterch, A., Grad, M., pi ák, A., Brückl, E., Hegedüs, E., Keller, G.R. and Thybo, H. 2003. Special Contribution: An Overview of Recent Seismic Refraction Experiments in Central Europe. *Studia geophysica et geodaetica*, **47**, 651-657, https://doi.org/10.1023/A:1024775921231

He, Z.-Y., Zhang, Z.-M., Zong, K.-Q. and Dong, X. 2013. Paleoproterozoic crustal evolution of the Tarim Craton: Constrained by zircon U–Pb and Hf isotopes of meta-igneous rocks from Korla and Dunhuang. *Journal of Asian Earth Sciences*, **78**, 54-70, https://doi.org/https://doi.org/10.1016/j.jseaes.2013.07.022

He, Z.-Y., Klemd, R., Yan, L.-L. and Zhang, Z.-M. 2018. The origin and crustal evolution of microcontinents in the Beishan orogen of the southern Central Asian Orogenic Belt. *Earth-Science Reviews*, **185**, 1-14, https://doi.org/https://doi.org/10.1016/j.earscirev.2018.05.012

He, Z., Zong, K., Jiang, H., Xiang, H. and Zhang, Z. 2014. Early Paleozoic tectonic evolution of the southern Beishan orogenic collage: Insights from the granitoids. *Acta Petrologica Sinica*, **30**, 2324-2338, [in Chinese with English abstract].

Horton, B.K., Dupont-Nivet, G., Zhou, J., Waanders, G.L., Butler, R.F. and Wang, J. 2004. Mesozoic-Cenozoic evolution of the Xining-Minhe and Dangchang basins, northeastern ~~Tibetan Plateau~~Tibetan Plateau: Magnetostratigraphic and biostratigraphic results. *Journal of Geophysical Research: Solid Earth*, **109**, https://doi.org/https://doi.org/10.1029/2003JB002913

Hu, P.-y., Zhai, Q.-g., Jahn, B.-m., Wang, J., Li, C., Lee, H.-y. and Tang, S.-h. 2015. Early Ordovician granites from the South Qiangtang terrane, northern Tibet: Implications for the early Paleozoic tectonic evolution along the Gondwanan proto-Tethyan margin. *Lithos*, **220-223**, 318-338, https://doi.org/https://doi.org/10.1016/j.lithos.2014.12.020

Huang, X., Gao, R., Li, W. and Xiong, X. 2021. Seismic reflection evidence of crustal duplexing and lithospheric underthrusting beneath the western Qilian Mountains, northeastern margin of the ~~Tibetan Plateau~~Tibetan Plateau. *Science China Earth Sciences*, **64**, 96-109, https://doi.org/10.1007/s11430-020-9677-y

HUANG, Z.-X., LI, H.-Y. and XU, Y. 2014. Lithospheric S-wave velocity structure of west China and neighboring areas from surface wave tomography. *Chinese Journal of Geophysics*, **57**, 3994-4004 [in Chinese with English abstract].

Jian, P., Kröner, A. *et al.* 2014. Zircon dating of Neoproterozoic and Cambrian ophiolites in West Mongolia and implications for the timing of orogenic processes in the central part of the Central Asian Orogenic Belt. *Earth-Science Reviews*, **133**, 62-93, https://doi.org/https://doi.org/10.1016/j.earscirev.2014.02.006

Kröner, A., Kovach, V. *et al.* 2014. Reassessment of continental growth during the accretionary history of the Central Asian Orogenic Belt. *Gondwana Research*, **25**, 103-125, https://doi.org/https://doi.org/10.1016/j.gr.2012.12.023

Lehmann, J., Schulmann, K. *et al.* 2010. Structural constraints on the evolution of the Central Asian Orogenic Belt in SW Mongolia. *American Journal of Science*, **310**, 575-628, https://doi.org/https://doi.org/10.2475/07.2010.02

Li, B., Qi, B. *et al.* 2023. Two-phase kinematic evolution of the Qilian Shan, northern ~~Tibetan Plateau~~Tibetan Plateau: Initial Eocene−Oligocene deformation that accelerated in the mid-Miocene. *Geological Society of America Bulletin*, https://doi.org/10.1130/B37159.1

Li, B., Zuza, A.V. *et al.* 2021. Corrigendum to Cenozoic multi-phase deformation in the Qilian Shan and out-of-sequence development of the northern ~~Tibetan Plateau~~Tibetan Plateau [Tectonophysics 782–783 (2020) 228423]. *Tectonophysics*, **808**, 228794, https://doi.org/https://doi.org/10.1016/j.tecto.2021.228794

Li, C., Wang, Q., Liu, X. and Tang, Y. 1982. *Explanatory notes to the tectonic map of Asia*. Geological Publishing House, Beijing [in Chinese with English abstract].

Li, G.-J., Wang, Q.-F., Huang, Y.-H., Gao, L. and Yu, L. 2016. Petrogenesis of middle Ordovician peraluminous granites in the Baoshan block: Implications for the early Paleozoic tectonic evolution along East Gondwana. *Lithos*, **245**, 76-92, https://doi.org/https://doi.org/10.1016/j.lithos.2015.10.012

Li, J., Wu, C. *et al.* 2022. Tectonic setting of metamorphism and exhumation of eclogite-facies rocks in the South Beishan orogen, northwestern China. *Geosphere*, **19**, 100-138, https://doi.org/10.1130/GES02548.1

Li, S., Huang, F. and Li, H. 2002. Post-collisional lithosphere delamination of the Dabie-Sulu orogen. *Chinese Science Bulletin*, **47**, 259-263, https://doi.org/10.1360/02tb9063

Liu, X. 1995. Tectonics of orogenic belts in Beishan Mts., western China and their evolution. *Dixue Yanjiu (Geosci. Research)*, **28**, 37-48 [in Chinese with English abstract].

Liu, Y., Yu, H., Xin, H., Lu, S., Xiu, Q. and Li, Q. 2009. Tectonic units division and Precambrian significant geological events in Altyn Tagh Mountain, China. *Geological Bulletin of China*, **28**, 1430-1438 [in Chinese with English abstract].

Lu, S., Li, H., Zhang, C. and Niu, G. 2008. Geological and geochronological evidence for the Precambrian evolution of the Tarim Craton and surrounding continental fragments. *Precambrian Research*, **160**, 94-107, https://doi.org/https://doi.org/10.1016/j.precamres.2007.04.025

Mei, H. 1998. Archean tonalite in the Dunhuang, Gansu Province: Age from the U-Pb single zircon and Nd isotope. *Process Precamb. Research*, **21**, 41-45 [in Chinese with English abstract].

Mei, H., Yu, H., Li, Q. and Zuo, G. 1997. Preliminary litho-tectonic framework of early Precambrian rocks in Dunhuang-Beishan area, Gansu, west China. *Progress in Precambrian Research*, **20**, 47-54, [in Chinese with English abstract].

Meng, Q.-R. 2003. What drove late Mesozoic extension of the northern China–Mongolia tract? *Tectonophysics*, **369**, 155-174, https://doi.org/https://doi.org/10.1016/S0040-1951(03)00195-1

Meyer, B., Tapponnier, P. *et al.* 1998. Crustal thickening in Gansu-Qinghai, lithospheric mantle subduction, and oblique, strike-slip controlled growth of the Tibet plateau. *Geophysical Journal International*, **135**, 1-47, https://doi.org/10.1046/j.1365-246X.1998.00567.x

Niu, W., Xin, H., Duan, L., Zhao, Z., Zhang, G., Ren, B. and Zhang, Y. 2020. Geochemical characteristics, zircon U-Pb age of SSZ ophiolite in the Baiheshan area of the Beishan orogenic belt, Inner Mongolia, and its indication for the evolution of the Paleo-Asian Ocean. *Geological Bulletin of China*, **39**, 1317-1329 [in Chinese with English abstract].

Pan, G.-t., Zhu, D.-c. and Wang, L.-q. 2004. Bangong Lake-Nu River suture zone-the northern boundary of Gondwanaland: Evidence from geology and geophysics. *Earth Science Frontiers*, **11**, 371-382 [in Chinese with English abstract].

Ren, J., Wang, Z. *et al.* 1999. The Tectonics of China from a Global View A Guide to the Tectonic Map of China and Adjacent Regions. *Beijing: Geol. Publ. House* [in Chinese with English abstract].

Şengör, A. 2015. The Founder of Modern Geology Died 100 Years Ago:: The Scientific Work and Legacy of Eduard Suess. *Geoscience Canada*, **42**, 181-246 [in Chinese with English abstract].

Shen, X., Li, Y. *et al.* 2020. Lateral growth of NE ~~Tibetan Plateau~~Tibetan Plateau restricted by the Asian lithosphere: Results from a dense seismic profile. *Gondwana Research*, **87**, 238-247, https://doi.org/https://doi.org/10.1016/j.gr.2020.06.018

Shi, M., Hou, Q., Wu, C., Yan, Q., Cheng, N., Zhang, Q.W.L. and Wang, H.Y.C. 2021. Origins of the meta-mafic rocks in the southern Dunhuang Block (NW China): Implication for tectonic framework of the southernmost Central Asian Orogenic Belt. *Geological Journal*, **56**, 3959-3973, https://doi.org/https://doi.org/10.1002/gj.4144

Shi, M., Hou, Q. *et al.* 2020. Paleozoic Sanweishan arc in the northern Dunhuang region, NW China: The Dunhuang block is a Phanerozoic orogen, not a Precambrian block. *Journal of Asian Earth Sciences*, **194**, 103954, https://doi.org/https://doi.org/10.1016/j.jseaes.2019.103954

Shi, Z., Gao, R., Lu, Z., Li, W., Li, H., Huang, X. and Liang, H. 2022. Bidirectional subduction of the Bangong-Nujiang ocean revealed by deep-crustal seismic reflection profile. *Tectonophysics*, **837**, 229455, https://doi.org/https://doi.org/10.1016/j.tecto.2022.229455

Song, D., Niu, G., Zhang, C. and Zhang, G. 2009. Time constraints on orogenesis from oceanic subduction to continental subduction, collision, and exhumation: An example from North Qilian and North Qaidam HP-UHP belts. *Acta Petrologica Sinica*, **25**, 2067-2077 [in Chinese with English abstract].

Song, D., Xiao, W., Han, C. and Tian, Z. 2014. Polyphase deformation of a Paleozoic forearc–arc complex in the Beishan orogen, NW China. *Tectonophysics*, **632**, 224-243, https://doi.org/https://doi.org/10.1016/j.tecto.2014.06.030

Song, D., Xiao, W., Windley, B.F., Han, C. and Tian, Z. 2015. A Paleozoic Japan-type subduction-accretion system in the Beishan orogenic collage, southern Central Asian Orogenic Belt. *Lithos*, **224-225**, 195-213, https://doi.org/https://doi.org/10.1016/j.lithos.2015.03.005

Song, S., Niu, Y., Su, L. and Xia, X. 2013. Tectonics of the North Qilian orogen, NW China. *Gondwana Research*, **23**, 1378-1401, https://doi.org/https://doi.org/10.1016/j.gr.2012.02.004

Tapponnier, P., Zhiqin, X., Roger, F., Meyer, B., Arnaud, N., Wittlinger, G. and Jingsui, Y. 2001. Oblique Stepwise Rise and Growth of the Tibet Plateau. *Science*, **294**, 1671-1677, https://doi.org/10.1126/science.105978

Tapponnier, P., Meyer, B. *et al.* 1990. Active thrusting and folding in the Qilian Shan, and decoupling between upper crust and mantle in northeastern Tibet. *Earth and Planetary Science Letters*, **97**, 382-403, https://doi.org/https://doi.org/10.1016/0012-821X(90)90053-Z

Vidale, J. 1988. Finite-difference calculation of travel times. *Bulletin of the Seismological Society of America*, **78**, 2062-2076, https://doi.org/10.1785/BSSA0780062062

Wang, C.-Y., Lou, H., Silver, P.G., Zhu, L. and Chang, L. 2010. Crustal structure variation along 30° in the eastern ~~Tibetan Plateau~~Tibetan Plateau and its tectonic implications. *Earth and Planetary Science Letters*, **289**, 367-376, [in Chinese with English abstract].

Wang, C., Deng, J., Lu, Y., Bagas, L., Kemp, A.I.S. and McCuaig, T.C. 2015. Age, nature, and origin of Ordovician Zhibenshan granite from the Baoshan terrane in the Sanjiang region and its significance for understanding Proto-Tethys evolution. *International Geology Review*, **57**, 1922-1939, https://doi.org/10.1080/00206814.2015.1043358

Wang, D., Luo, L., Tang, Y., Yin, F., Wang, B., Wang, L. and Center, C. 2016. Zircon U-Pb dating and petrogenesis of Early Paleozoic adakites from the Niujingshan ophiolitic mélange in the Changning-Menglian suture zone and its geological implications. *Acta Petrologica Sinica*, **32**, 2317-2329 [in Chinese with English abstract].

Wang, H.Y.C., Wang, J. *et al.* 2017. Metamorphic evolution and geochronology of the Dunhuang orogenic belt in the Hongliuxia area, northwestern China. *Journal of Asian Earth Sciences*, **135**, 51-69, https://doi.org/https://doi.org/10.1016/j.jseaes.2016.12.014

Wang, Q. and Liu, X. 1981. Qilian Mountains Caledonian Polycyclic Double Metamorphic Belt. *Collection of papers on the geotectonics of China and its neighboring regions Beijing: Geological Publishing House*, 92-101 [in Chinese with English abstract].

Wang, S., Zhang, K., Song, B., Li, S., Li, M. and Zhou, J. 2018. Geochronology and geochemistry of the Niujuanzi ophiolitic mélange, Gansu Province, NW China: implications for tectonic evolution of the Beishan Orogenic Collage. *International Journal of Earth Sciences*, **107**, 269-289, https://doi.org/10.1007/s00531-017-1489-2

Wang, T., Huang, H. *et al.* 2022. Voluminous continental growth of the Altaids and its control on metallogeny. *National Science Review*, **10**, https://doi.org/10.1093/nsr/nwac283

Wang, W., Zheng, D. *et al.* 2020. Cenozoic Exhumation of the Qilian Shan in the Northeastern ~~Tibetan Plateau~~Tibetan Plateau: Evidence From Low ‐ Temperature Thermochronology. *Tectonics*, **39** [in Chinese with English abstract].

Wang, Z., Xiong, X., Wu, G., Li, Z., Ye, Z. and Jin, Z. 2023. Crustal structure and deformation mechanism of the western northeast ~~Tibetan Plateau~~Tibetan Plateau. *Frontiers in Earth Science*, **11**, https://doi.org/10.3389/feart.2023.1255813

Wei, X., Jiang, M., Liang, X., Chen, L. and Ai, Y. 2017. Limited southward underthrusting of the

Asian lithosphere and material extrusion beneath the northeastern margin of Tibet, inferred from teleseismic Rayleigh wave tomography. *Journal of Geophysical Research: Solid Earth*, **122**, 7172-7189, https://doi.org/https://doi.org/10.1002/2016JB013832

Wei, Z., Huang, Z., Jin, X., Sun, Y. and Huo, J. 2004. Geological characteristics of ophiolite migmatitic complex of Hongshishan region, Gansu. *Northwest Geol*, **37**, 13-18 [in Chinese with English abstract].

Wu, C., Yin, A., Zuza, A.V., Zhang, J., Liu, W. and Ding, L. 2016. Pre-Cenozoic geologic history of the central and northern ~~Tibetan Plateau~~Tibetan Plateau and the role of Wilson cycles in constructing the Tethyan orogenic system. *Lithosphere*, **8**, 254-292, https://doi.org/10.1130/L494.1

Wu, C., Gao, Y. *et al.* 2011. An early Palaeozoic double-subduction model for the North Qilian oceanic plate: evidence from zircon SHRIMP dating of granites. *International Geology Review*, **53**, 157-181, https://doi.org/10.1080/00206810902965346

Wu, C., Zuza, A.V. *et al.* 2017. Geochronology and geochemistry of Neoproterozoic granitoids in the central Qilian Shan of northern Tibet: Reconstructing the amalgamation processes and tectonic history of Asia. *Lithosphere*, **9**, 609-636, https://doi.org/10.1130/L640.1

Wu, G., Xiong, X. *et al.* 2022. 2D Tomographic imaging of the P-wave velocity structure in the upper crust beneath the southern Beishan tectonic belt. *Earth Science Frontiers*, **29**, 402-415, https://doi.org/10.13745/j.esf.sf.2022.2.2

Xiao, Q., Zhang, J., Wang, J., Zhao, G. and Tang, J. 2012. Electrical resistivity structures between the Northern Qilian Mountains and Beishan Block, NW China, and tectonic implications. *Physics of the Earth and Planetary Interiors*, **200-201**, 92-104, https://doi.org/https://doi.org/10.1016/j.pepi.2012.04.008

Xiao, Q., Shao, G., Yu, G., Cai, J. and Wang, J. 2016. Electrical resistivity structures of the Kunlun–Qaidam–Qilian system at the northern Tibet and their tectonic implications. *Physics of the Earth and Planetary Interiors*, **255**, 1-17, https://doi.org/https://doi.org/10.1016/j.pepi.2016.03.011

Xiao, Q., Yu, G., Liu-Zeng, J., Oskin, M.E. and Shao, G. 2017. Structure and geometry of the Aksay restraining double bend along the Altyn Tagh Fault, northern Tibet, imaged using magnetotelluric method. *Geophysical Research Letters*, **44**, 4090-4097, https://doi.org/https://doi.org/10.1002/2017GL072581

Xiao, W., Windley, B.F., Yong, Y., Yan, Z., Yuan, C., Liu, C. and Li, J. 2009. Early Paleozoic to Devonian multiple-accretionary model for the Qilian Shan, NW China. *Journal of Asian Earth Sciences*, **35**, 323-333, https://doi.org/https://doi.org/10.1016/j.jseaes.2008.10.001

Xiao, W., Windley, B.F. *et al.* 2018. Late Paleozoic to early Triassic multiple roll-back and oroclinal bending of the Mongolia collage in Central Asia. *Earth-Science Reviews*, **186**, 94-128, https://doi.org/https://doi.org/10.1016/j.earscirev.2017.09.020

Xiao, W., Qigui, M. *et al.* 2010. Paleozoic multiple accretionary and collisional processes of the Beishan orogenic collage. *American Journal of Science*, **310**, 1553-1594, https://doi.org/10.2475/10.2010.12]

Xin, H., Niu, W., Tian, J., Teng, X. and Duan, X. 2020. Spatio-temporal structure of Beishan orogenic belt and evolution of Paleo-Asian Ocean, Inner Mongolia. *Geological Bulletin of China*, **39**, 1297-1316 [in Chinese with English abstract].

Xiong, Z.-Q., Qian, W., Suzuki, K. and O. McNamara, J. 2003. Formation of Complement Membrane Attack Complex in Mammalian Cerebral Cortex Evokes Seizures and Neurodegeneration. *The Journal of Neuroscience*, **23**, 955, https://doi.org/10.1523/JNEUROSCI.23-03-00955.2003

Xu, Q., Pei, S., Yuan, X., Zhao, J., Liu, H., Tu, H. and Chen, S. 2019. Seismic Evidence for Lateral Asthenospheric Flow Beneath the Northeastern ~~Tibetan Plateau~~Tibetan Plateau Derived From S Receiver Functions. *Geochemistry, Geophysics, Geosystems*, **20**, 883-894, https://doi.org/https://doi.org/10.1029/2018GC007986

Xu, X.-Y., Xia, L.-Q. and Xia, Z.-C. 2005. Volcanism and mineralization in the North Qilian Orogenic Belt, Northwestern China. Springer Berlin Heidelberg, Berlin, Heidelberg, 487-489. https://doi.org/10.1007/3-540-27946-6_126

Xu, Z., Yang, J., Zhang, J., Jiang, M., Li, H. and Cui, J. 1999. A comparison between the tectonic units on the two sides of the Altun sinistral strike-slip fault and the mechanism of lithospheric shearing. *Acta Geologica Sinica*, **73**, 193-205 [in Chinese with English abstract].

Yang, H., Xiong, S., Liu, Q., Zhou, D., Yang, X., Fan, Z. and Jia, Z. 2024. Tectonic framework of Qilian orogen: reveal from an aeromagnetic anomaly feature. *Applied Geophysics*, https://doi.org/10.1007/s11770-023-1041-z

Yang, H., Li, Y. *et al.* 2010. Character and structural attribute of the Beishan ophiolite. *Northwestern Geology*, **43**, 26-36 [in Chinese with English abstract].

Yang, H., Yang, X. *et al.* 2019. Quaternary Activity of the Beihewan Fault in the Southeastern Beishan Wrench Belt, Western China: Implications for Crustal Stability and Intraplate Earthquake

Hazards North of Tibet. *Journal of Geophysical Research: Solid Earth*, **124**, 13286-13309, https://doi.org/https://doi.org/10.1029/2018JB017209

Yin, A. and Harrison, T.M. 2000. Geologic Evolution of the Himalayan-Tibetan Orogen. *Annual Review of Earth and Planetary Sciences*, **28**, 211-280, https://doi.org/doi:10.1146/annurev.earth.28.1.211

Yu, H., Mei, H. and Li, Q. 1998. The characteristics of Archean khondalite series in Dunhuang, Gansu Province. *Progress in Precambrian Research*, **21**, 19-25 [in Chinese with English abstract].

Yu, J., Li, X., Wang, G., Wu, P. and Yan, Q. 2012. Zircon U-Pb ages of Huitongshan and Zhangfangshan ophiolite in Beishan of Gansu-Inner Mongolia border area and their significance. *Geological Bulletin of China*, **31**, 2038-2045 [in Chinese with English abstract].

Yu, S., Peng, Y. *et al.* 2021. Tectono-thermal evolution of the Qilian orogenic system: Tracing the subduction, accretion and closure of the Proto-Tethys Ocean. *Earth-Science Reviews*, **215**, 103547, https://doi.org/https://doi.org/10.1016/j.earscirev.2021.103547

Yuan, D.-Y., Ge, W.-P. *et al.* 2013. The growth of northeastern Tibet and its relevance to large-scale continental geodynamics: A review of recent studies. *Tectonics*, **32**, 1358-1370, https://doi.org/https://doi.org/10.1002/tect.20081

Yuan, Y., Zong, K. *et al.* 2015. Geochemical and geochronological evidence for a former early Neoproterozoic microcontinent in the South Beishan Orogenic Belt, southernmost Central Asian Orogenic Belt. *Precambrian Research*, **266**, 409-424, https://doi.org/https://doi.org/10.1016/j.precamres.2015.05.034

Yue, Y. and Liou, J.G. 1999. Two-stage evolution model for the Altyn Tagh fault, China. *Geology*, **27**, 227-230, https://doi.org/10.1130/0091-7613(1999)027<0227:TSEMFT>2.3.CO;2

Yun, L., Zhang, J. *et al.* 2021. Discovery of active faults in the southern Beishan area, NW China: implications for regional tectonics. *Journal of Geomechanics*, **27**, 195-207 [in Chinese with English abstract].

Zelt, C.A. and Smith, R.B. 1992. Seismic traveltime inversion for 2-D crustal velocity structure. *Geophysical Journal International*, **108**, 16-34, https://doi.org/10.1111/j.1365-246X.1992.tb00836.x

Zhang, J. and Cunningham, D. 2012. Kilometer-scale refolded folds caused by strike-slip reversal and intraplate shortening in the Beishan region, China. *Tectonics*, **31**, https://doi.org/https://doi.org/10.1029/2011TC003050

Zhang, J., Cunningham, D. *et al.* 2021. Kinematic variability of late Cenozoic fault systems and contrasting mountain building processes in the Alxa block, western China. *Journal of Asian Earth Sciences*, **205**, 104597, https://doi.org/https://doi.org/10.1016/j.jseaes.2020.104597

Zhang, J., Zhang, B. *et al.* 2023. Late Cenozoic deformation characteristics and mechanism of the Beishan-Alxa region. *Earth Science Frontiers*, **30**, 334 [in Chinese with English abstract].

Zhang, P.-Z., Molnar, P. and Xu, X. 2007. Late Quaternary and present-day rates of slip along the Altyn Tagh Fault, northern margin of the ~~Tibetan Plateau~~Tibetan Plateau. *Tectonics*, **26**, https://doi.org/https://doi.org/10.1029/2006TC002014

Zhang, Z., Deng, Y., Teng, J., Wang, C.-Y., Gao, R., Chen, Y. and Fan, W. 2011. An overview of the crustal structure of the ~~Tibetan Plateau~~Tibetan Plateau after 35 years of deep seismic soundings. *Journal of Asian Earth Sciences*, **40**, 977-989, https://doi.org/10.1016/j.jseaes.2010.03.010

Zhang, Z., Xin, H. *et al.* 2020. The discovery of the Elegen ophiolite in Beishan orogenic belt, Inner Mongolia: Evidence for the east extension of the Hongshishan-Baiheshan ophiolite belt. *Geological Bulletin of China*, **39**, 1389-1403 [in Chinese with English abstract].

Zhao, G., Wu, Z., Liu, J., Zhang, L. and Zuo, J. 2019. The time space distribution characteristics and migration law of large earthquakes in the Indiam-Eurasian plate collision deformation area. *Journal of Geomechanics*, **25**, 324-340 [in Chinese with English abstract].

Zhao, G., Wang, Y., Huang, B., Dong, Y., Li, S., Zhang, G. and Yu, S. 2018. Geological reconstructions of the East Asian blocks: From the breakup of Rodinia to the assembly of Pangea. *Earth-Science Reviews*, **186**, 262-286, https://doi.org/https://doi.org/10.1016/j.earscirev.2018.10.003

Zhao, L., Li, Y. *et al.* 2024. Geochronology and geochemistry of early Paleozoic magmatism in the Qilian orogen: Constraints on closure of the Proto-Tethys Ocean. *Gondwana Research*, **126**, 223-242, https://doi.org/https://doi.org/10.1016/j.gr.2023.10.006

Zheng, D., Wang, W. *et al.* 2017. Progressive northward growth of the northern Qilian Shan–Hexi Corridor (northeastern Tibet) during the Cenozoic. *Lithosphere*, **9**, 408-416, https://doi.org/10.1130/l587.1

Zheng, Y., Zhang, Q. *et al.* 1996. Great Jurassic thrust sheets in Beishan (North Mountains)—Gobi areas of China and southern Mongolia. *Journal of Structural Geology*, **18**, 1111-1126, https://doi.org/https://doi.org/10.1016/0191-8141(96)00038-7

Zong, K., Liu, Y., Zhang, Z., He, Z., Hu, Z., Guo, J. and Chen, K. 2013. The generation and evolution of Archean continental crust in the Dunhuang block, northeastern Tarim craton, northwestern

China. *Precambrian Research*, **235**, 251-263, https://doi.org/https://doi.org/10.1016/j.precamres.2013.07.002

Zuo, G. and Liu, J. 1987. The evolution of tectonic of Early Paleozoic in North Qilian range, China. *Chinese Journal of Geology*, **22**, 14-24 [in Chinese with English abstract].

Zuo, G. and Li, S. 2011. Early Paleozoic tectonic framework and evolution in the northeast margin of Tarim Basin. *GEOLOGY IN CHINA*, **38**, 945-960 [in Chinese with English abstract].

Zuo, G., Zhang, S., He, G. and Zhang, Y. 1991. Plate tectonic characteristics during the early paleozoic in Beishan near the Sino-Mongolian border region, China. *Tectonophysics*, **188**, 385-392, https://doi.org/https://doi.org/10.1016/0040-1951(91)90466-6

Zuza, A.V., Cheng, X. and Yin, A. 2016. Testing models of ~~Tibetan Plateau~~Tibetan Plateau formation with Cenozoic shortening estimates across the Qilian Shan–Nan Shan thrust belt. *Geosphere*, **12**, 501-532, https://doi.org/10.1130/GES01254.1

Zuza, A.V., Wu, C., Wang, Z., Levy, D.A., Li, B., Xiong, X. and Chen, X. 2019. Underthrusting and duplexing beneath the northern ~~Tibetan Plateau~~Tibetan Plateau and the evolution of the Himalayan-Tibetan orogen. *Lithosphere*, **11**, 209-231, https://doi.org/10.1130/L1042.1

Zuza, A.V., Wu, C. *et al.* 2017. Tectonic evolution of the Qilian Shan: An early Paleozoic orogen reactivated in the Cenozoic. *GSA Bulletin*, **130**, 881-925, https://doi.org/10.1130/B31721.1

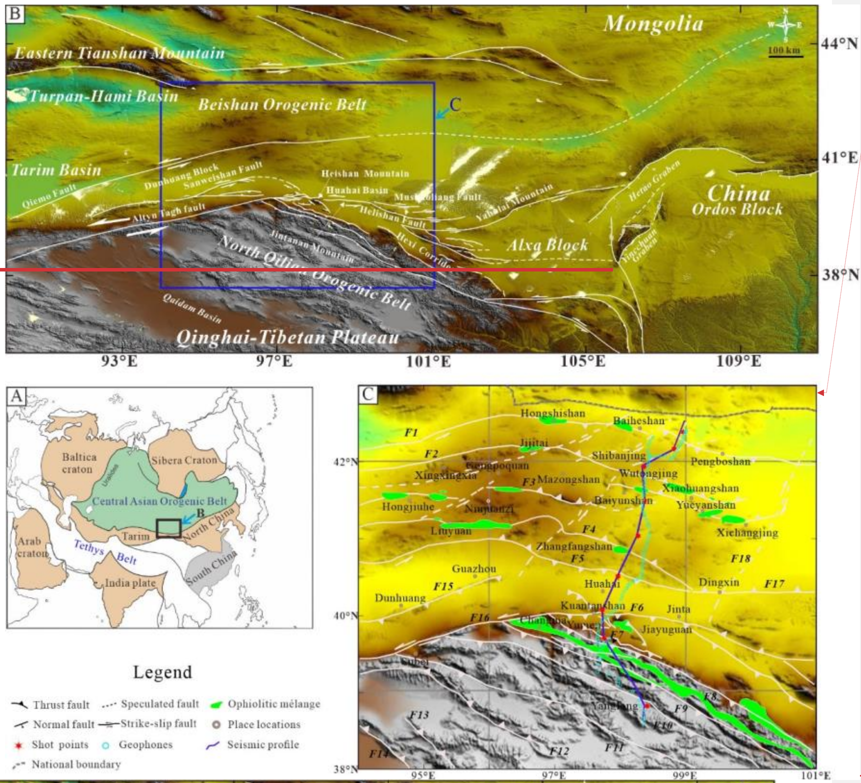

带格式的: 正文

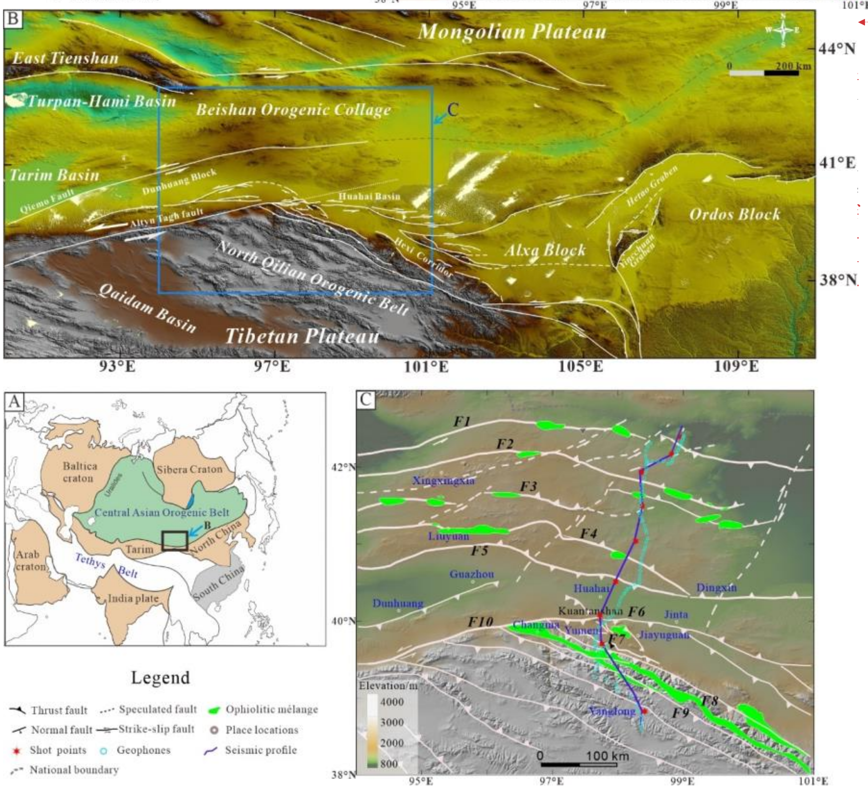

带格式的: 缩进: 首行缩进: 0 厘米

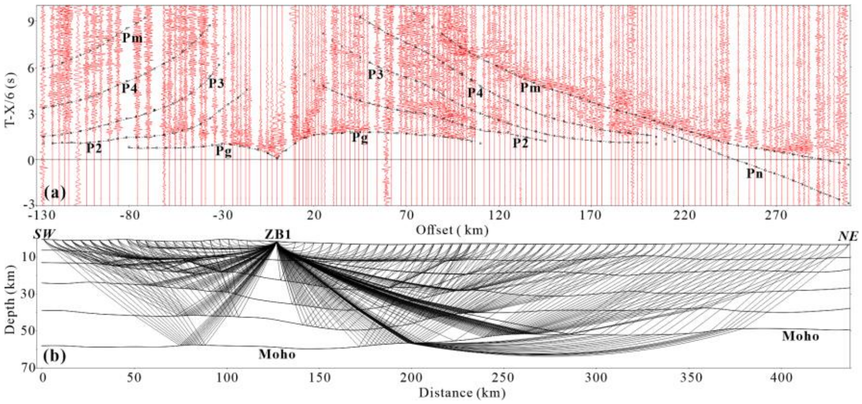

Fig. 2 P-wave record section (on a reduced time scale) corresponding to the shot point ZB1 and identified seismic phases. The seismic phases are marked by dotted lines, and the squares mark the location of calculated traveltimes.

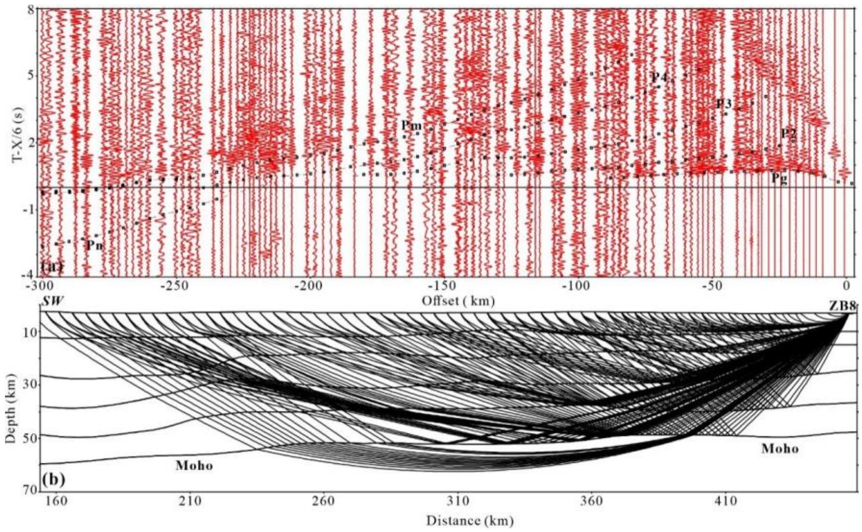

Fig. 3 P-wave record section (on a reduced time scale) corresponding to the shot point ZB8 and identified seismic phases. The seismic phases are marked by dotted lines, and the squares indicate the location of calculated traveltimes.

带格式的: 段落间距段后: 0 磅, 行距: 单倍行距

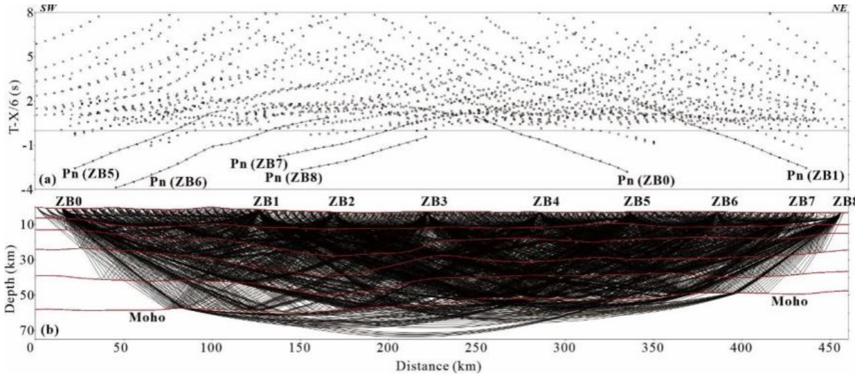

Fig. 4 Traveltime fitting and ray coverage of all shots. (a) ray tracing coverage of the model; (b) rays of all the phases for nine shots.

带格式的: 段落间距段后: 0 磅, 行距: 单倍行距

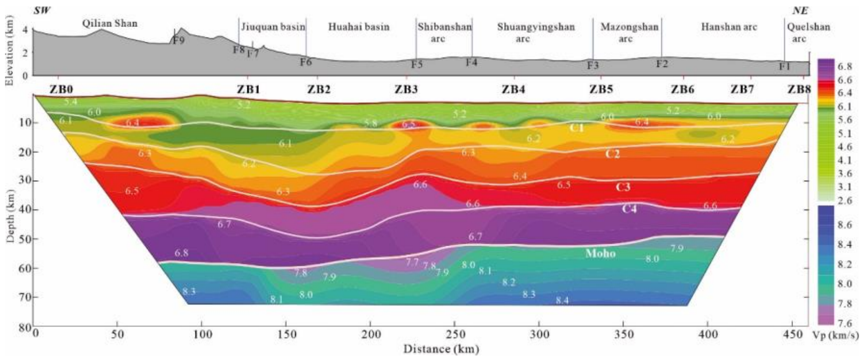

Fig. 5 2-D crustal-upper mantle velocity structure; (a) Topography showing main tectonic units; (b) crustal-upper mantle velocity structure. White solid lines denote the main interfaces resolved from wide-angle reflections.

带格式的: 段落间距段后: 0 磅, 行距: 单倍行距

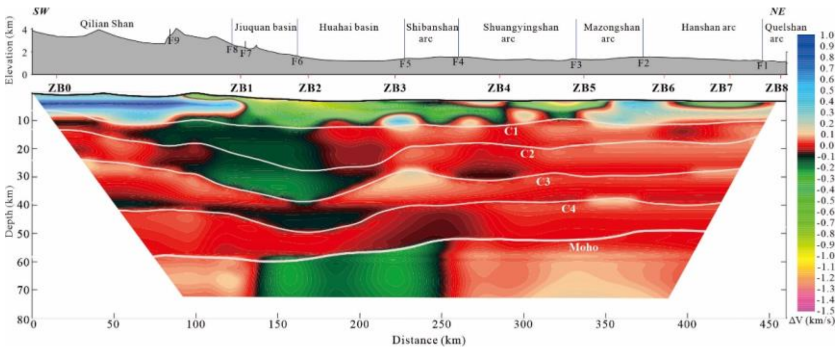

Fig. 6 2-D crustal- upper mantle velocity anomal~~it~~y structure (layer means subtracted from velocities shown in Fig. 5); (a) Topography showing the main tectonic units; (b) crustal-upper mantle velocity anomal~~it~~y structure. White solid lines denote the main interfaces.

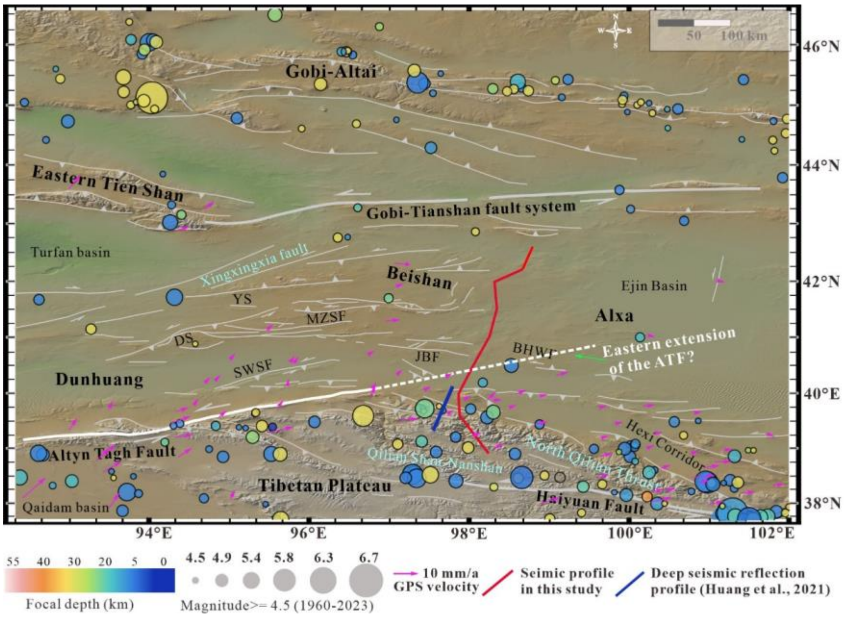

Fig. 7 Earthquake distribution, GPS motion direction, and velocity in ~~NE Tibet~~The NE Tibetan Plateau and the ~~Beishan block~~ Beishan Orogenic Collage (modified from Yang et al., 2021). Purple arrows indicate GPS vectors relative to stable Siberia. The dashed white line indicates the proposed eastern extension of the ATF. BHWF: Beihewan Fault; JJF: Jiujing fault system; MZSF: Mazongshan fault system; SWSF: Sanweishan Fault; DS: Daquan Shan; YS: Yushi Shan.

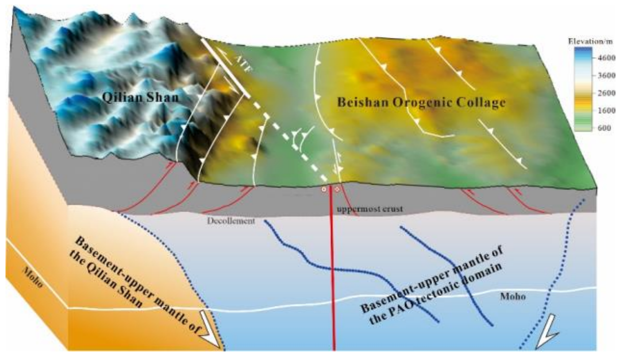

Fig. 8 Tectonic interpretations of ~~observed~~ features derived from~~in~~ the velocity model ~~in~~ across the North Qilian–Beishan- Orogenic Collage~~area~~. Blue dotted lines ~~represent~~ indicate the inferred subduction directions of the fossil subduction slabs. -Red solid lines denote the faults imaged at depth, whereas the white solid and dashed lines represent surface fault traces~~Faults (F1-F8) align with Fig.1~~.

带格式的: 段落间距段后: 0 磅, 行距: 单倍行距

Table 1 Explosion position of the deep seismic sounding profile

Shot No.	Longitude (° E)	Latitude (° N)	Elevation (m)	TNT charge (kg)	Shot time (UTC+8)
ZB0	98.406	38.825	3387	2000	00:00:04.900
ZB1	97.761	39.702	2466	2000	23:59:46.890
ZB2	97.724	40.074	1447	2000	23:01:44.285
ZB3	97.965	40.512	1334	1500	22:04:11.157
ZB4	98.271	41.038	1302	1500	22:01:44.340
ZB5	98.367	41.495	1341	2000	22:00:13.350
ZB6	98.364	41.937	1520	3000	23:00:27.270
ZB7	98.818	42.172	1243	2000	20:05:02.438
ZB8	98.958	42.387	1154	3000	23:03:05.596

Table 2 The RMS error of traveltime fitting for different seismic phases

Shot	Pg		P2		P3		P4		Pm		Pn	
	No. of picks	RMS time (s)	No. of picks	RMS time (s)	No. of picks	RMS time (s)	No. of picks	RMS time (s)	No. of picks	RMS time (s)	No. of picks	RMS time (s)
ZB0	16	0.0251	26	0.0137	33	0.0169	37	0.0144	47	0.0159	17	0.0127
ZB1	58	0.021	58	0.02	57	0.0268	57	0.0207	75	0.0248	26	0.0265
ZB2	52	0.0309	46	0.032	46	0.0238	55	0.0244	51	0.0266	17	0.0275
ZB3	48	0.0157	60	0.0226	61	0.0144	59	0.0158	44	0.0123		
ZB4	35	0.0274	39	0.0216	36	0.0218	39	0.0351	35	0.0206		
ZB5	31	0.0118	29	0.0108	43	0.0191	34	0.0189	48	0.0225	13	0.0204
ZB6	33	0.0228	36	0.0155	37	0.0254	41	0.0204	61	0.0218	19	0.0256
ZB7	32	0.0246	29	0.019	31	0.0221	33	0.0197	48	0.018	21	0.0238
ZB8	28	0.0309	25	0.033	33	0.0233	55	0.0228	53	0.0272	12	0.0228
Mean RMS time (s)		0.0234		0.0209		0.0215		0.0214		0.0211		0.0227
Total picks	333		348		377		410		462		125	

带格式的: 缩进: 首行缩进: 0 厘米
设置了格式: 英语(美国)
设置了格式: 英语(美国)
带格式的: 左
带格式的: 左
带格式的: 左
设置了格式: 英语(美国)
带格式的: 左
设置了格式: 英语(美国)
带格式的: 左
设置了格式: 英语(美国)
带格式的: 左
设置了格式: 英语(美国)
带格式的: 左
设置了格式: 英语(美国)
带格式的: 左
设置了格式: 英语(美国)
带格式的: 左
设置了格式: 英语(美国)
带格式的: 左
设置了格式: 英语(美国)
带格式的: 左
设置了格式: 英语(美国)
带格式的: 左
设置了格式: 英语(美国)
带格式的: 左
设置了格式: 英语(美国)